A search for large-scale effects of ship emissions on clouds and radiation in satellite data

K. Peters,[1] J. Quaas,[2] and H. Graßl[1]

Received 7 July 2011; revised 26 October 2011; accepted 27 October 2011; published 30 December 2011.

[1] Ship tracks are regarded as the most obvious manifestations of the effect of anthropogenic aerosol particles on clouds (indirect effect). However, it is not yet fully quantified whether there are climatically relevant effects on large scales beyond the narrow ship tracks visible in selected satellite images. A combination of satellite and reanalysis data is used here to analyze regions in which major shipping lanes cut through otherwise pristine marine environments in subtropical and tropical oceans. We expect the region downwind of a shipping lane is affected by the aerosol produced by shipping emissions but not the one upwind. Thus, differences in microphysical and macrophysical cloud properties are analyzed statistically. We investigate microphysical and macrophysical cloud properties as well as the aerosol optical depth and its fine-mode fraction for the years 2005–2007 as provided for by retrievals of the two Moderate Resolution Imaging Spectroradiometer instruments. Water-cloud properties include cloud optical depth, cloud droplet effective radius, cloud top temperature, and cloud top pressure. Large-scale meteorological parameters are taken from ERA-Interim reanalysis data and microwave remote sensing (sea surface temperature). We analyze the regions of interest in a Eulerian and Lagrangian sense, i.e., sampling along shipping lanes and sampling along wind trajectories, respectively. No statistically significant impacts of shipping emissions on large-scale cloud fields could be found in any of the selected regions close to major shipping lanes. In conclusion, the net indirect effects of aerosols from ship emissions are not large enough to be distinguishable from the natural dynamics controlling cloud presence and formation.

Citation: Peters, K., J. Quaas, and H. Graßl (2011), A search for large-scale effects of ship emissions on clouds and radiation in satellite data, *J. Geophys. Res.*, *116*, D24205, doi:10.1029/2011JD016531.

1. Introduction

[2] In this study, we aim at analyzing effects of shipping emissions on the properties of oceanic liquid water clouds at a large scale by means of satellite derived quantities.

[3] Seagoing ships are one of the least regulated sources of anthropogenic emissions, often burning low-quality residual fuels containing high amounts of sulfur or even heavy metals. Besides gaseous compounds such as carbon dioxide and carbon monoxide (CO_2, CO), nitrous oxides (NO_x), methane (CH_4) and nonmethane hydrocarbons (NMHCs), combustion of such fuels produces large amounts of aerosols and aerosol precursors. These come in form of particulate matter (PM) consisting of elemental (black) and organic carbon, sulfate, ash and particles forming from sulfuric acid [e.g., *Eyring et al.*, 2005; *Petzold et al.*, 2008]. Where these aerosols are mixed into clouds within the marine boundary layer (MBL), a certain number of emitted particles can serve as cloud condensation nuclei (CCN) [*Hobbs et al.*, 2000; *Petzold et al.*, 2005; *Dusek et al.*, 2006; *Petzold et al.*, 2008], leading to aerosol indirect effects (AIEs). In the past decades, a whole suite of AIE hypotheses has been put forward of which the "Twomey effect," or first AIE, is the most prominent. For this effect, an increase in available CCN eventually leads to more and smaller cloud droplets if the liquid water content of the respective cloud remains constant. More cloud droplets increase the total droplet surface area by which the cloud albedo is enhanced; an effect which in principle had been formulated in the literature as early as the 1940s [e.g., *Hewson*, 1943] and put into the general context of anthropogenic pollution by *Twomey* [1974]. Other AIE hypotheses include effects on cloud lifetime [*Albrecht*, 1989; *Small et al.*, 2009] or cloud top height [*Koren et al.*, 2005; *Devasthale et al.*, 2005; *Teller and Levin*, 2006]. Especially the latter hypotheses are far from being verified [e.g., *Stevens and Feingold*, 2009]. In total, AIEs are subject to the largest uncertainties of all radiative forcing (RF) components of the Earth system, when it comes to assessing human-induced climate change [*Forster et al.*, 2007].

[4] Moreover, the emitted aerosols and aerosol precursor gases also lead to aerosol direct radiative effects (DREs), i.e., the aerosol particles absorb and scatter the incident

[1]Max-Planck-Institut für Meteorologie, Hamburg, Germany.
[2]Institute for Meteorology, University of Leipzig, Leipzig, Germany.

0148-0227/11/2011JD016531

solar radiation directly [*Ångström*, 1962; *McCormick and Ludwig*, 1967]. While regionally, a warming effect by aerosol absorption can be substantial [e.g., *Peters et al.*, 2011], globally, aerosol DREs are believed to exert a net radiative cooling at the top of the atmosphere (TOA), thereby dampening the overall global warming by anthropogenic greenhouse gas emissions [*Haywood and Boucher*, 2000; *Forster et al.*, 2007]. The global averaged DRE of shipping emissions is small and estimated to range from -47.5 to -9.1 m Wm^{-2} [*Eyring et al.*, 2010] but its quantification is not the subject of this paper.

[5] AIEs from shipping emissions are manifested in linear cloud structures referred to as "ship tracks" and these were first observed in satellite imagery by *Conover* [1966]. There, the author hypothesized that ship effluents provided additional CCN which lead to the more reflective clouds; a theory which has attained increasing support from observational efforts [e.g., *Hobbs et al.*, 2000; *Petzold et al.*, 2005; *Langley et al.*, 2010]. Later, *Twomey et al.* [1968] followed up on that work, highlighting the importance of clean maritime environments for the ship tracks to form and become visible and thereby also delivering a first stepping stone toward the principle of "cloud susceptibility" [e.g., *Platnick and Twomey*, 1994]. Therefore, the first encounters with ship emissions' influence on clouds provided the basis for the discovery of basic AIE principles.

[6] Over the past decades, the use of ship tracks as a test bed for the study of AIEs has inspired many observational studies [e.g., *Coakley et al.*, 1987; *Radke et al.*, 1989; *Platnick and Twomey*, 1994]. In the Monterey Area Ship Track (MAST) experiment [*Durkee et al.*, 2000], a considerable amount of ship tracks, along with the large-scale meteorological environment, was observed in the stratocumulus decks off the coast of California.

[7] With more advanced satellite observational capabilities becoming available, the focus of the latest ship track studies is more concerned with the statistical characterization of the ship tracks on local and global scales. These studies illustrated that it is essential to take both the microphysical and macrophysical properties of polluted clouds into account to explain an apparent change in visible cloud optical depth τ. *Coakley and Walsh* [2002] investigated several hundred ship tracks and found that the obtained increase in τ was much too small in relation to the change in cloud droplet effective radius r_{eff}. Assuming a reduction of the cloud liquid water path (LWP) in the polluted clouds then provided the missing link in radiative transfer calculations. These findings were confirmed by *Segrin et al.* [2007] and *Christensen et al.* [2009] who both investigated the stratocumulus decks off the coast of California with morning and afternoon satellite measurements of the MODIS instrument.

[8] This decrease of LWP in clouds polluted by ship effluents is not confirmed by other studies, though. In their data sample, *Lu et al.* [2007] found the LWP of a cloud polluted by ship emissions to increase while the LWP of the other clouds in the sample was reduced with increasing aerosol number concentration. Most probably, the sampling of clouds persisting in different large-scale meteorological conditions leads to these differences. Indeed, recent studies [e.g., *Stevens and Feingold*, 2009] have suggested investigating aerosol indirect effects by cloud regime. *Christensen and Stephens* [2011] have in fact most recently investigated the effect of ship emissions on clouds in different dynamical regimes: closed-cell and open-cell cloud regimes showed similar microphysical but different macrophysical responses. Whereas the LWP is reduced and cloud top height (CTH) remains unchanged for the closed-cell regime, LWP and CTH both increase for the open-cell regime. The fractional contribution of microphysical and macrophysical effects to the change in τ is also estimated: in closed and open cells, the microphysical and macrophysical changes dominate the increase in τ, respectively.

[9] *Christensen and Stephens* [2011] also found that ship tracks persist over several hours in stratocumulus decks and thereby confirmed earlier results by *Schreier et al.* [2010] who used geostationary satellite measurements to derive the diurnal cycle of ship tracks off the coast of southern Africa. In this region, the ship tracks' appearance yielded a maximum in the late morning hours and the general ship track characteristics were found to be similar to the ones measured in MAST [*Durkee et al.*, 2000].

[10] Studies of ship track occurrence on a global scale with satellite observations was, to our knowledge, performed by two studies. *Schreier et al.* [2007] used 1 year data to compile a global statistic of ship tracks identified by visual analysis, whereas *Campmany et al.* [2009] utilized an automatic ship track detection algorithm. Both studies find accumulations of ship tracks over similar regions of the worlds' oceans with the exception that *Campmany et al.* [2009] did not find any tracks off the coast of Africa (an updated version of the algorithm also finds some tracks off the coast of Africa (A. M. Sayer, personal communication, 2011)). Putting ship tracks into the climate context, *Schreier et al.* [2007] also made an attempt to estimate the TOA radiative forcing of observed ship tracks and find it to be about -0.4 to -0.6 m Wm^{-2}. More recently, A. M. Sayer and R. G. Grainger (Ship tracks: Modification of cloud properties and radiative forcing estimate from ATSR-2 data, submitted to *Meteorologische Zeitschrift*, 2011) came up with a value of -8.9 m Wm^{-2} where the difference to the results of *Schreier et al.* [2007] can be explained by different approaches for characterizing the atmospheric background.

[11] The above-mentioned studies all focus on the detection and characterization of ship tracks. Nevertheless, it is very well acknowledged that shipping emissions significantly alter the MBL aerosol composition over global oceans, especially in the Northern Hemisphere. By this, shipping emissions have the potential to change the microphysical and macrophysical properties of cloud fields also at a large, climatically relevant, scale. The investigation of these large-scale effects of shipping emissions needs special attention and should utilize approaches which use data from numerical models and/or satellite instrument measurements.

[12] Concerning the satellite part of this recommendation, there is a study which has investigated ship emission influence on cloud fields: *Devasthale et al.* [2006] looked at the statistical properties of low clouds over European coastal waters and found evidence of cloud property modification through shipping emissions in the heavily frequented area of the English Channel. From a chemistry point of view, *Richter et al.* [2004] and *Marbach* [2009] used satellite data to detect an influence of shipping emissions on atmospheric NO_2 and formaldehyde concentrations, respectively.

[13] So far, only the modeling perspective of the above recommendation has been seriously followed in a number of studies. These utilize general circulation models (GCMs) to quantify the effect of shipping emissions on clouds on a global scale [*Capaldo et al.*, 1999; *Lauer et al.*, 2007, 2009]. Some of these studies compute AIEs from shipping emissions with a global mean radiative forcing at the top of the atmosphere as large as -0.6 Wm^{-2}. These effects are mainly confined to the low cloud areas west of the continents, but can also be found in the storm tracks of the North Atlantic and Pacific oceans. As the present estimate of the total greenhouse gas (GHG) radiative forcing, as given by the IPCC, is about +3 Wm^{-2}, these model results suggest that AIEs from shipping might mask a significant portion of the GHG-induced radiative forcing. With the International Maritime Organizations' (IMO) regulation on the reduction of the sulfur content of marine bunker fuel coming into force within the next decade [*International Maritime Organization*, 1998], the magnitude of the negative TOA RF from ship-induced AIEs may be bound to decrease in spite of a global increase of ship traffic [*Lauer et al.*, 2009].

[14] In this study, we propose a new approach toward assessing the effect of ship emissions on clouds. We aim at sampling clean and polluted maritime regions of similar large-scale meteorology. We then collect properties of clouds and aerosols retrieved from satellite measurements as well as information on the local meteorology to quantify the overall scenes. Then we perform a statistical analysis of the acquired data with respect to clean and polluted environments in order to isolate an effect of shipping emissions on cloud properties. The satellite data used in this study are described in section 2 and the general methodology is illustrated in section 3. We then present the results of two analysis approaches in sections 4 and 5 and a discussion and summary in section 6.

2. Data

[15] We use cloud and aerosol properties as well as sea surface temperature retrieved from satellite observations, using instruments mounted on the EOS Aqua and EOS Terra polar-orbiting satellites. EOS Aqua flies in an ascending orbit with an equator crossing time of 13:30 UTC, whereas EOS Terra flies in a descending orbit with an equator crossing time of 10:30 UTC.

2.1. Clouds, Aerosols, and Radiation

[16] We use highly resolved cloud and aerosol properties retrieved from both the Moderate Resolution Imaging Spectroradiometer (MODIS) instruments. Concerning cloud properties, we use τ, r_{eff}, cloud top temperature (CTT), cloud top pressure (CTP), LWP and cloud fraction [*Platnick et al.*, 2003]. Because we are interested in just low-level liquid water clouds and want to avoid as many retrieval errors as possible, we filter the MODIS Level 2 data to consider only (1) confidently cloudy pixels, (2) liquid water phase, and (3) single-layer clouds as obtained from the MODIS quality assurance flags. Furthermore, to avoid ambiguities in the retrieved cloud microphysical quantities, we only use pixels in which $\tau > 4$ and $r_{\mathrm{eff}} < 20$ μm [*Nakajima and King*, 1990; *Platnick et al.*, 2003]. By applying this filtering, we discard about 30%–70% of available data and find mean low-level cloud fraction >0.96 at pixel level (similar to the study of *Kotarba* [2010]). We compute the cloud droplet number concentration (CDNC) for liquid clouds from r_{eff} and τ assuming adiabaticity [*Quaas et al.*, 2006]. Concerning the calculation of CDNC, we acknowledge that the adiabatic assumption breaks down for broken cloud fields [e.g., *Hayes et al.*, 2010], but we are confident in applying that assumption to our data because the cloudy pixels that pass the quality filtering are very close to overcast.

[17] To characterize the aerosol population, we use aerosol optical depth (AOD) and the fine-mode fraction (FMF) of the AOD as retrieved from MODIS data. The FMF quantifies the part of the AOD which corresponds to particles in the submicron size range and is mostly associated with anthropogenic combustion aerosol [*Remer et al.*, 2005; *Bellouin et al.*, 2008]. All the above parameters are taken from the MODIS Collection 5 Joint Level 2 products (MODATML2, MYDATML2). We take large-scale liquid cloud fraction from the MODIS Collection 5 Level 3 products (MYD08_D3, MOD08_D3).

[18] To characterize the radiative properties at the top of the atmosphere (TOA) for the regions of interest, we take data acquired from the Clouds and the Earth's Radiant Energy System (CERES) [*Wielicki et al.*, 1996; *Loeb and Manalo-Smith*, 2005] instrument and collected in the Level 2 single-scanner footprint (SSF) product. We only use the spectrally integrated (0.3–5 μm) upwelling shortwave radiative flux at TOA. From this, we calculate the local planetary albedo by relating the outgoing shortwave flux to the incoming solar radiation which we compute by use of the solar zenith angle of the measurement scene at the surface, the eccentricity of Earth's orbit and a solar constant of 1365 Wm^{-2} as used in the CERES retrievals. The CERES Single Scanner Footprint (SSF) product offers a spatial resolution of about $0.25° \times 0.25°$.

2.2. Meteorological Environment

[19] We characterize the local meteorological environment using both satellite and reanalysis data. We use sea surface temperature (SST) as retrieved from measurements by the Advanced Microwave Scanning Radiometer Earth Observing System (AMSR-E) instrument, which is mounted on EOS Aqua, to sample for the conditions in the lowermost troposphere. The root-mean-square retrieval error of the SST is estimated at $\pm$0.58°C [*Wentz and Meissner*, 2000], but we assume this error to average out due to the large sample size (on the order of several thousand). Additional meteorological parameters are taken from the ERA-Interim Reanalysis data set [*Simmons et al.*, 2007]. We use local noon for both Aqua and Terra, assuming that this model output time is sufficient to characterize the local meteorology for both satellite overpass times. The used parameters are wind speed and direction at 10 m height as well as the boundary layer height (BLH). We also take ERA-Interim data to calculate the lower tropospheric stability (LTS) according to *Klein and Hartmann* [1993]. The ERA-Interim data are provided at $1.5° \times 1.5°$ spatial resolution. From the retrieved MODIS CTT and AMSR-E SST, we also compute an approximate cloud top height (CTH) assuming a constant lapse rate of -6.5 K km^{-1}, take this as a proxy for BLH and compare it to the BLH as retrieved from ERA-Interim.

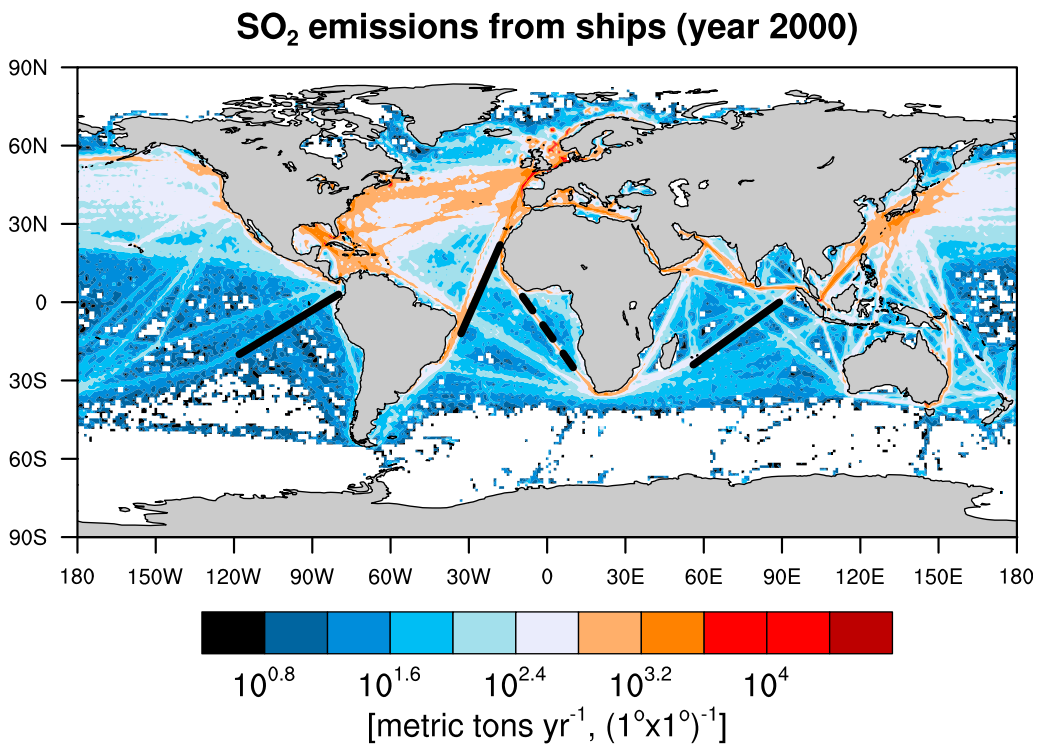

Figure 1. Geographical distribution of total annual SO_2 emissions from ships in the emission data set of Behrens (2006). Color coding is for the $\log_{10}$ of total emissions in metric tons per year. The black lines indicate the three shipping lanes in otherwise unpolluted marine environments selected for analysis. The dashed line shows a shipping lane excluded from analysis (see section 4).

2.3. Ship Emission Inventory

[20] We use the shipping emission inventory presented by H. L. Behrens (Present traffic and emissions from maritime shipping, in Deliverable D1.1.2.2 of the EU-IP QUANTIFY, Det Norske Veritas, 2006; hereinafter referred to as Behrens, 2006), representative for the year 2000 (see Figure 1) for the definition of shipping lanes which cut through otherwise pristine marine environments. In this inventory, the geographical distribution of shipping emissions is obtained by the using a combination Comprehensive Ocean–atmosphere Data Set (COADS) and Automatic Mutual-Assistance Vessel Rescue System (AMVER) ship traffic densities for the years 2000 and 2001–2002, respectively. COADS is maintained by the NOAA (National Oceanic and Atmospheric Administration) and is a publicly available data set of global marine surface observations. These include ship positions and ship identifiers reported by oceangoing vessels on a voluntary basis, which can then be used for allocation of shipping emissions. AMVER is a ship reporting system on a voluntary basis to aid the rescue of people in distress at sea. This system is generally constrained to ships having of size larger than 1000 gross tonnage (GT), but *Endresen et al.* [2003] illustrate that the AMVER ship position data set very well represents the global cargo fleet. To distribute the annual emissions in the inventory presented by (2006), 997168 (COADS) and 993074 (AMVER) marine reports were used as input for deriving global ship reporting frequencies as illustrated by *Endresen et al.* [2003]. The global distributions of ship reporting frequencies are shown by *Dalsøren et al.* [2009].

3. General Methodology

[21] In this study we aim at quantifying the effect of shipping emissions on clouds via a statistical analysis of satellite data. The time frame of the study is 2005–2007, and we analyze environments over the open oceans at a large scale. We try to detect an effect of shipping emissions on large-scale cloud fields, including situations in which ship tracks cannot readily be observed. Our approach therefore differs from previous satellite data based studies on the influence of ship emissions on clouds, because these focused on clearly visible ship tracks.

[22] Although the change in cloud properties may not be obvious from just looking at the single cloud fields, we expect the cloud properties in polluted regions to show on average different microphysical and macrophysical properties from the clouds observed in cleaner regions, if aerosol indirect effects from ship emissions are significant at a large scale. The main hurdle in this approach is the clear definition of clean and polluted regions which still show a comparable large-scale meteorology in such a way that part of the "cloud problem," i.e., the uncertain relationship between the statistics of a cloud field and ambient meteorological conditions, can be eliminated [*Stevens and Feingold*, 2009].

[23] We propose that a definition of clear and polluted regions is feasible with the combination of ship emission inventories and reanalysis data: if a shipping lane leads

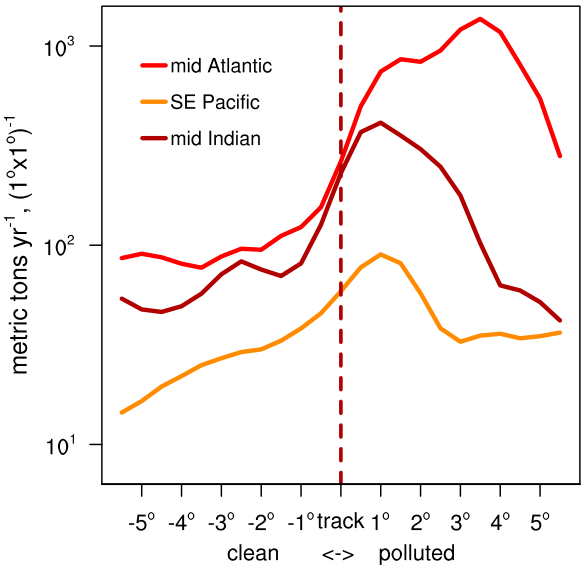

Figure 2. Total annual SO_2 emissions across selected corridors in Figure 1 (log_{10} scale) as a function of distance from the shipping lane (units of degree), sampled according to 10 m wind direction.

through an otherwise largely unpolluted region and if there is a mean low-level wind blowing across this shipping lane, then we expect the air mass downwind of the shipping lane to be affected by the pollution from the ship emissions, but not the air mass upwind of the shipping lane. Going in hand with the diversity of AIE hypotheses, the microphysical and macrophysical cloud properties in the polluted region should then be different from those in the clean region. Then, if statistically significant, this would reveal a climatically relevant effect of shipping emissions on large-scale cloud fields and subsequently radiation. It is important to note that we are not able to sample for individual ship movements, i.e., we cannot discriminate between those scenes which are polluted and those which are unpolluted.

[24] In terms of notation in this paper, the terms "shipping corridor" or "corridor" refer to the respective regions of interest including the defined shipping lane as well as the clean and polluted regions upwind and downwind of the shipping lane, respectively.

[25] We select regions which are subject to large spatial contrast in shipping emissions by visual analysis of a ship emission inventory (see section 2.3). Also, the regions should not be situated too close to continental landmasses to avoid aerosol contamination from continental pollution, and the regions should not be subject to significant seasonal variation in wind direction, such as monsoonal circulation patterns. Regions were selected based on the emission profiles across the associated shipping lanes as shown in Figure 2. As the focus of this study is on the influence of shipping emissions on clouds, we show 3 year (2005–2007) mean values of water cloud fraction as retrieved by MODIS (Aqua) in Figure 3 for the shipping corridors in the southeast Pacific, mid Atlantic and mid Indian oceans as illustrated in Figure 1.

[26] We define the region which is upwind of the respective track as "clean" and the region which is downwind of the track as "polluted." We use the 10 m wind direction as provided by the ERA-Interim Reanalysis to identify the areas upwind and downwind of the ship track. To account for efficient vertical mixing in the boundary layer, we compared the wind directions at 925 hPa (≈700 m) to those at 10 m and found no distinct differences. In the selected regions, the local meteorology, especially the lower tropospheric winds, does not vary very much with time. Therefore, the regions which are defined as clean and polluted, respectively, remain the same most of the time. For example, the region south of the shipping lane in the southeast Pacific is usually clean (Figure 3, middle), whereas the region north of this shipping lane is usually polluted because winds are mostly southeasterly in this region. The same methodology applies for the shipping corridor in the mid Indian Ocean (Figure 3, right). In the mid-Atlantic region (Figure 3, left), the boundary layer winds are mostly easterly. Therefore most of the time the area eastward of the shipping lane is

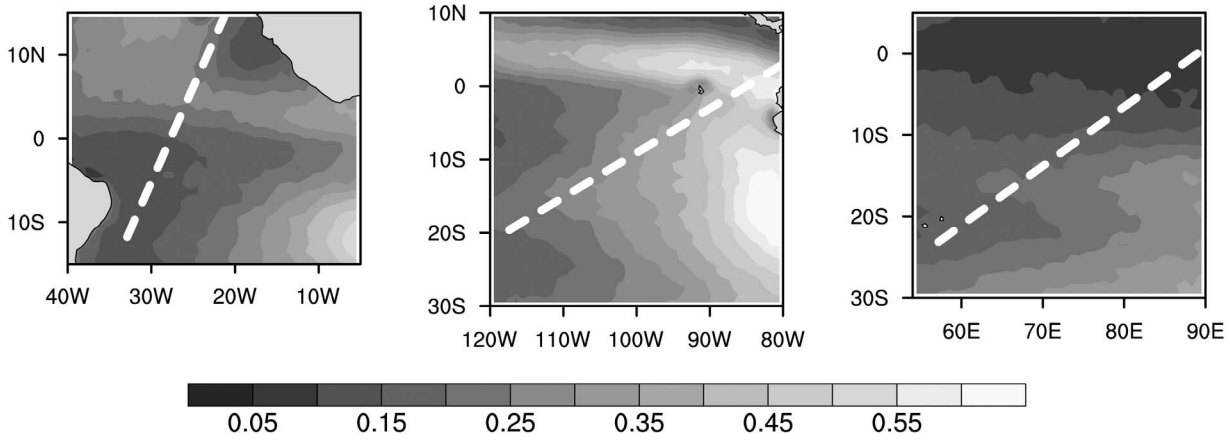

Figure 3. Three year (2005–2007) mean water cloud fraction as derived from operational MODIS (Aqua) Collection 5 Level 3 data for the (left) regions in the mid Atlantic, (middle) southeast Pacific, and (right) mid Indian oceans. The dashed white lines indicate the position of the windward edge of the shipping lanes analyzed in each region.

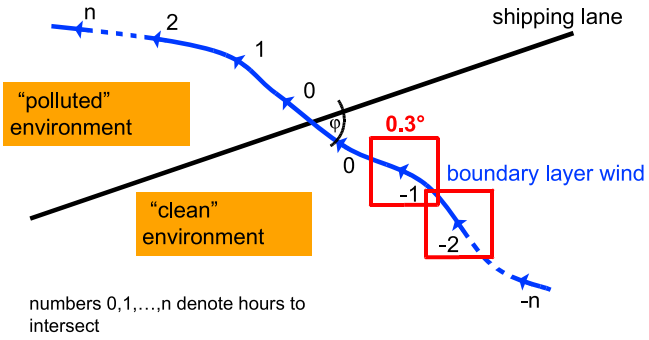

Figure 4. Conceptual illustration of the Lagrangian analysis concept (not to scale).

clean and the area westward of the shipping lane is polluted with respect to shipping emissions. The across-corridor emission profiles shown in Figure 2 illustrate the change in emissions at the point of the defined shipping lane.

[27] We have developed two analysis strategies which should allow one to determine changes in cloud properties due to shipping emissions. One approach follows a Lagrangian strategy whereas the other approach follows a Eulerian strategy. We show the method and results of the Lagrangian approach in section 4 whereas the method and results of the Eulerian approach are shown in section 5.

[28] Again a note on the notation in this paper: when we speak in words similar to "changes near the intersect," we refer to the area within ≈200 km of the intersect (±2° for the Eulerian approach and 5 h for the Lagrangian approach).

4. Lagrangian Approach

4.1. Method

[29] The general approach to perform a Lagrangian analysis to quantify the effect of shipping emissions on clouds is illustrated in Figure 4. Using wind trajectory analysis (following *Sandu et al.* [2010]), we can identify wind trajectories which intersect a predefined shipping lane. Then, we can distinguish clean and polluted parts of each wind trajectory: the part of the trajectory prior to ("upwind") the intersection with the shipping lane is considered clean, whereas the part after ("downwind") is considered polluted. We hypothesize that cloud microphysical properties are different between the clean and polluted parts, due to the effect of shipping emissions. Analyzing satellite data along a given wind trajectory should then reveal different cloud properties for the clean and polluted parts of the respective trajectory.

[30] We select three shipping lanes for our Lagrangian analysis: (1) the shipping lane from the Panama Canal to Australia, (2) the shipping lane from the southern African tip northwestward, and (3) the mid-Atlantic part of the shipping lane from Europe to South America. The selected regions are depicted in Figure 5.

[31] Second, we analyze low-level wind trajectories in these regions to find scenes in which the boundary layer air masses cross the respective shipping lane. We use wind trajectories which are calculated using the Hybrid Single-Particle Lagrangian Integrated Trajectory (HYSPLIT) model (http://ready.arl.noaa.gov/HYSPLIT.php). The trajectories for shipping lanes 1 and 2 are a subset of those used by *Sandu et al.* [2010]. For the analysis of lane 3, we compute low-level wind trajectories analogous to the method described by *Sandu et al.* [2010]: the wind trajectories are initialized at 200 m height from nine equally spaced points inside a grid box having latitude and longitude coordinates of the possible permutations from (2S, 5S, 8S) and (15W, 18W, 21W), respectively. These starting points are chosen to ensure that the wind trajectories cross the shipping lane as shown in Figure 5. We are interested in whether or not a given wind trajectory intersects one of the prescribed shipping lanes. We therefore calculate the intersection point of each given wind trajectory by means of linear algebra. This intersection point and the respective trajectory is classified as useful for further analysis if (1) the height of the trajectory does not exceed 500 m above sea level 15 h before and 15 h after the intersection and (2) the intersection angle is 90° ± 80°. The number of useful scenes with respect to intersection angle

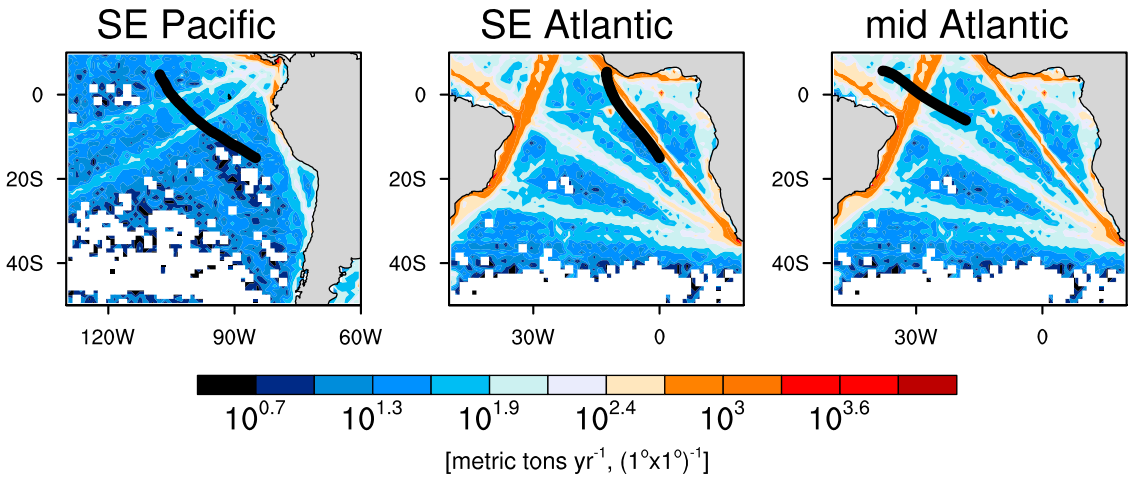

Figure 5. Application of the Lagrangian analysis concept. Contours show SO_2 emissions from ships as described by Behrens (2006, Figure 1). The black lines indicate the mean low-level wind trajectories for the region of interest (2002–2007).

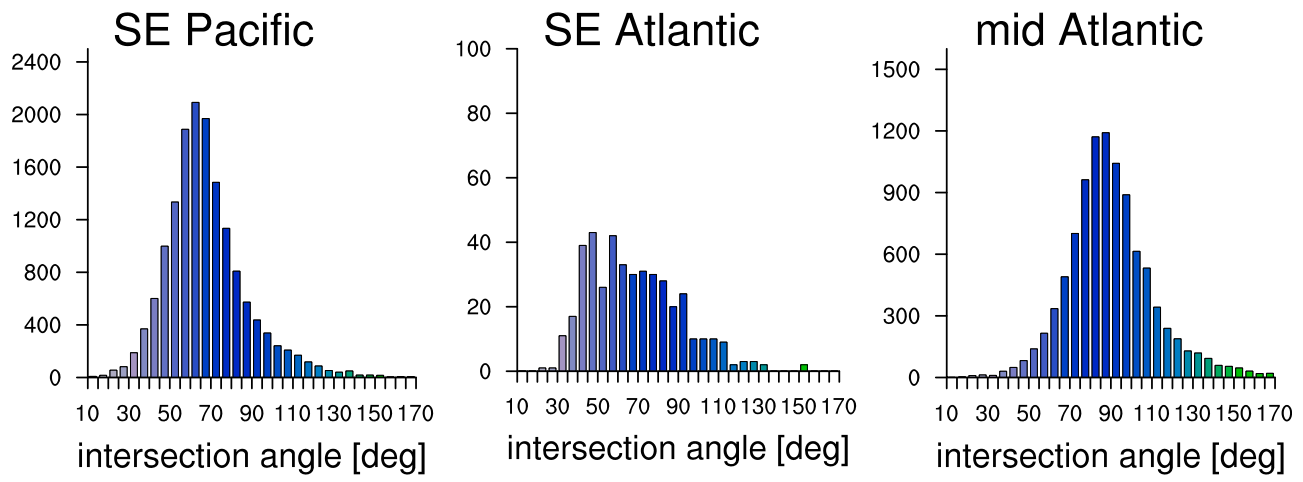

Figure 6. Number of useful scenes (as defined in section 4.1) for each of the regions of interest. The number of measurements is given as the function intersection angle between the shipping lane and the trajectory. The total number of useful scenes is 15408, 427, and 9816 for the southeast Pacific, southeast Atlantic, and mid-Atlantic regions, respectively.

for each region is given in the histograms shown in Figure 6. The amount of useful scenes for the southeastern Atlantic Ocean (Figure 5, middle) is relatively small because in that region, most of the calculated wind trajectories are almost parallel to the shipping lane. Because the low number of useful scenes does not allow for sound statistics, we exclude that region from our further analysis.

[32] Third, we analyze aerosol and cloud properties along the useful trajectories. We do not use all trajectories categorized as "useful" by the above analysis, but only those whose intersection times fall within a time window which matches the satellite overpass times. We define these time windows as 10:00–17:00 UTC for the mid-Atlantic region and 14:00–22:00 UTC for the southeast (SE) Pacific region. After applying this time window filter, the number of useful trajectories is 3284 for the SE Pacific and 2486 for the mid-Atlantic region. Because the trajectory model delivers hourly output of trajectory locations, we are able to sample for satellite data at every hour of the trajectory. We restrict our analysis to the trajectory locations 15 h before and 15 h after the intersect with the shipping lane. The 15 h before and the 15 h after the intersect will from now on be termed as "clean" and "polluted" areas, respectively. Satellite data are analyzed for a $0.3° \times 0.3°$ grid box which is centered around a given trajectory point (as illustrated in Figure 4). All valid satellite pixels within a $0.3° \times 0.3°$ box for a particular observation time are averaged to represent a daily average. This leads to 15 daily averages (one for each hourly trajectory position) for each of the two parts of the wind trajectory ("clean" or "polluted"). The results are then averaged for all trajectories crossing the respective shipping lane, which gives a long-term mean value for each hourly trajectory position. Because the obtained parameter distributions are not normally distributed, we estimate the error separately for observations having larger/smaller values than the respective mean value: the mean upper/lower difference to the mean value is divided by $\sqrt{N}$, with N being the number of daily averages for the $0.3° \times 0.3°$ hourly trajectory bins with values larger/smaller than the mean of each bin.

4.2. Results

4.2.1. Southeast Pacific Region

[33] We show the results of the wind trajectory analysis for the SE Pacific region in Figure 7 as a function of time to the calculated intersect with the shipping lane. We find an increase in the SST of about 0.5 K, a reduction of the LTS of about 1.2 K and a reduction of the BLH by about 140 m along the mean wind trajectory. Thus, although the MBL gets slightly more unstable along the trajectories, BLH as diagnosed from the reanalysis as well as the BLH proxy from MODIS CTT is reduced; the BLH proxy suggests a substantially higher MBL, though, which is also consistent with the results of *Wood and Bretherton* [2004].

[34] Along the mean trajectory, the number of MODIS pixels valid for analysis per $0.3° \times 0.3°$ averaging domain is slightly reduced for the cloudy scenes, but stays about constant for pixels having valid aerosol retrievals. The retrieved cloud and aerosol properties mostly show the same patterns for both MODIS instruments. If applicable, we explicitly mention differences in the following. The retrieved AOD shows a slight and rather constant increase along the trajectories with the ones retrieved from MODIS (Terra) having an offset from the ones retrieved from MODIS (Aqua) (this is a known issue of MODIS Collection 5) [*Remer et al.*, 2008]. The retrieved FMF shows increasing values for both instruments, with the values retrieved from MODIS (Terra) being substantially higher than the ones from MODIS (Aqua) (which is on the order of the oceanic background level) [*Remer et al.*, 2008]. This is interesting because the slight increase in the FMF could indicate an influence of shipping emissions on MBL aerosol composition. The calculated CDNC also increases and for the LWP, the retrievals by the two instruments lead to different along-trajectory gradients: the LWP slightly decreases for MODIS (Terra) and slightly increases for MODIS (Aqua). Although these changes appear systematic, the relative change is only on the order of 3%. In combination with the retrieved gradients in AOD, FMF and CDNC, the data retrieved from both instruments could indicate a first aerosol effect. But we also obtain a

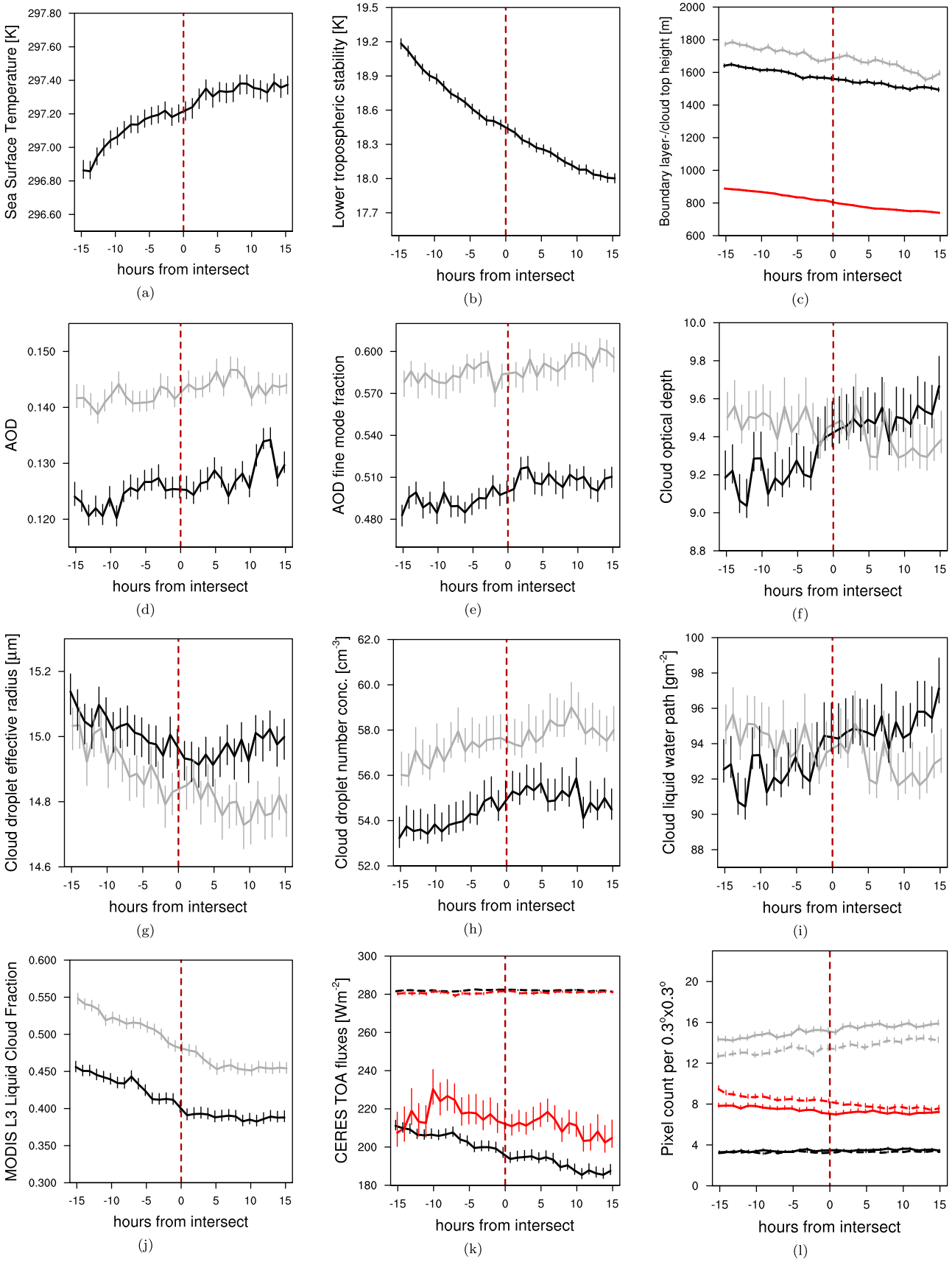
Sea Surface Temperature [K]
hours from intersect
(a)
Lower tropospheric stability [K]
hours from intersect
(b)
Boundary layer-/cloud top height [m]
hours from intersect
(c)
AOD
hours from intersect
(d)
AOD fine mode fraction
hours from intersect
(e)
Cloud optical depth
hours from intersect
(f)
Cloud droplet effective radius [µm]
hours from intersect
(g)
Cloud droplet number conc. [cm-3]
hours from intersect
(h)
Cloud liquid water path [gm-2]
hours from intersect
(i)
MODIS L3 Liquid Cloud Fraction
hours from intersect
(j)
CERES TOA fluxes [Wm-2]
hours from intersect
(k)
Pixel count per 0.3°x0.3°
hours from intersect
(l)

Figure 7

reduction of CTH, manifested in both the BLH proxy from retrieved CTTs as well as decreasing cloud top pressure (CTP, not shown; derived from a combination of MODIS-measured brightness temperatures and NCEP reanalysis data) [*Platnick et al.*, 2003]. Assuming an adiabatic cloud droplet effective radius (r_{eff}) profile, the retrieved along-trajectory decrease of r_{eff} values is consistent with the reduced CTHs.

[35] Thus, the apparent change in calculated CDNC may have its cause in cloud dynamics, which outweighs any arguments advocating the first AIE as it is just of second-order importance for cloud formation and properties (with the first-order influence given by the thermodynamic structure and natural aerosol concentration of the ambient air mass) [e.g., *Houze*, 1994; *Pruppacher and Klett*, 1997]. Furthermore, evidence of shipping emissions in the retrieved aerosol properties is essential for concluding an observed first indirect effect. But we obtain no systematic change in retrieved AOD and its FMF near the intersect with the shipping lane. The obtained increases of both properties is most probably associated with the oceanic background aerosol concentrations and we therefore also do not find a direct aerosol effect (DRE) due to shipping emissions.

[36] Although our measurement setup allows for reducing the influence of meteorological variability, such as distinct seasonal and interannual changes in the large-scale circulation, we cannot avoid the sampling along a gradient of increasing SSTs. As we are interested in low liquid water clouds residing in or slightly above the MBL, the mean cloud top characteristics of these clouds are bound to be affected by the slight change in SST along the trajectories. This is reflected in the retrieved gradients of low-level cloud fraction. The TOA radiative fluxes as retrieved from CERES (Aqua) correlate well with the retrieved cloud fraction gradients: the shortwave part decreases in along-trajectory direction and there is no indication of a distinct change near the intersect. It is therefore not possible to isolate a microphysical effect of shipping emissions on clouds, and therefore on the TOA radiation budget from our statistical analysis for the region investigated.

4.2.2. Mid-Atlantic Region

[37] We show the results from the wind trajectory analysis for the shipping lane in the mid-Atlantic region as a function of time from the intersect in Figure 8. The sea surface temperature as retrieved from the AMSR-E instrument increases by about 0.2 K, the LTS decreases slightly by about 0.1 K and the boundary layer height as retrieved from the reanalysis decreases by about 60 m along the trajectories. However, the BLH proxy using MODIS-retrieved CTTs shows substantially higher values and also increases along the mean trajectory. As shown for the SE Pacific region, the results for the BLH proxy most probably represent the MBL height more closely. Therefore, the increase in SST results in a slight destabilization of the lower troposphere which in turn leads to an increase in BLH and CTH. This is also confirmed by reduced CTP (not shown).

[38] For the MODIS-retrieved cloud and aerosol properties, the two sensors show similar along-trajectory gradients with MODIS (Terra) values mostly slightly higher than the ones from MODIS (Aqua). The number of valid pixels available for analysis is approximately the same for both cloud and aerosol properties. This implies that our filtering for useful pixels discards a substantial amount of potentially cloudy pixels because these are available at 5×5 km^2 resolution, whereas aerosol properties are available at 10×10 km^2. We find a steady increase in AOD along the wind trajectories by about 10%, but the FMF is about constant throughout the mean trajectory. As for the SE Pacific region, thus, ship emission aerosols are not distinguishable in the column aerosol concentrations as represented by the retrieved AOD, which also implies that there is no aerosol DRE of shipping emissions in this region. The calculated mean CDNC and LWP are also approximately constant in along-trajectory direction which reflects no distinct change in r_{eff} and τ in along-trajectory direction. Thus, no first indirect effect is visible either. We do find systematic gradients in more macrophysical cloud field properties though: the cloud fraction increases by about 4% and CTP decreases by about 20 hPa (not shown). So for the trajectories analyzed in this region, the mean large-scale cloud fraction slightly increases and the increase in CTH matches the reduced LTS values in along-trajectory direction. The retrieved TOA radiative fluxes also show no distinct change near the intersection point but match the gradient in cloud fraction: shortwave fluxes increase and longwave fluxes decrease in along-trajectory direction.

[39] Therefore, although we find an increase of AOD on the order of 10% in along-trajectory direction, there is no evidence of an influence of shipping emission on either the properties of the MBL aerosol composition or on the properties of low-level liquid water clouds in this region. Nevertheless, large-scale cloud field properties like the mean CTH and cloud fraction show distinct gradients; these can be explained by the gradient in the meteorological conditions, i.e., the increase in SSTs and subsequent destabilization of the lower troposphere.

5. Eulerian Approach

5.1. Method

[40] For the Eulerian perspective, we average along straight lines which we define parallel to the respective shipping lane. These have the same length as the shipping lane and are shifted in equal steps orthogonal to the shipping

Figure 7. Three year mean values of the Lagrangian trajectory analysis for the southeast Pacific region aerosol and cloud parameters: (a) SST; (b) LTS; (c) boundary layer and cloud top height derived from ERA-Interim (red) and MODIS cloud top temperatures (black, gray), respectively; (d) AOD; (e) AOD fine-mode fraction (FMF); (f) τ; (g) r_{eff}; (h) CDNC; (i) LWP; (j) cloud fraction; (k) outgoing southwest and LW fluxes, and (l) pixel count statistics for each $0.3° \times 0.3°$ box. For Figures 7c–7j, the black and gray curves represent data from MODIS on Aqua and Terra, respectively. In Figure 7k, the solid and dashed curves represent the reflected shortwave and outgoing longwave fluxes from CERES; black and red denote all-sky and cloudy-sky values, respectively. In Figure 1, the red and black lines show valid cloud and aerosol retrievals, respectively; gray denotes invalid pixels with respect to cloud filtering; solid and dashed lines denote retrievals from Aqua and Terra, respectively. The error bars denote the confidence in the calculated mean value toward higher/lower values (see section 3). The curves are shifted with respect to each other along the x axis to avoid overlapping.

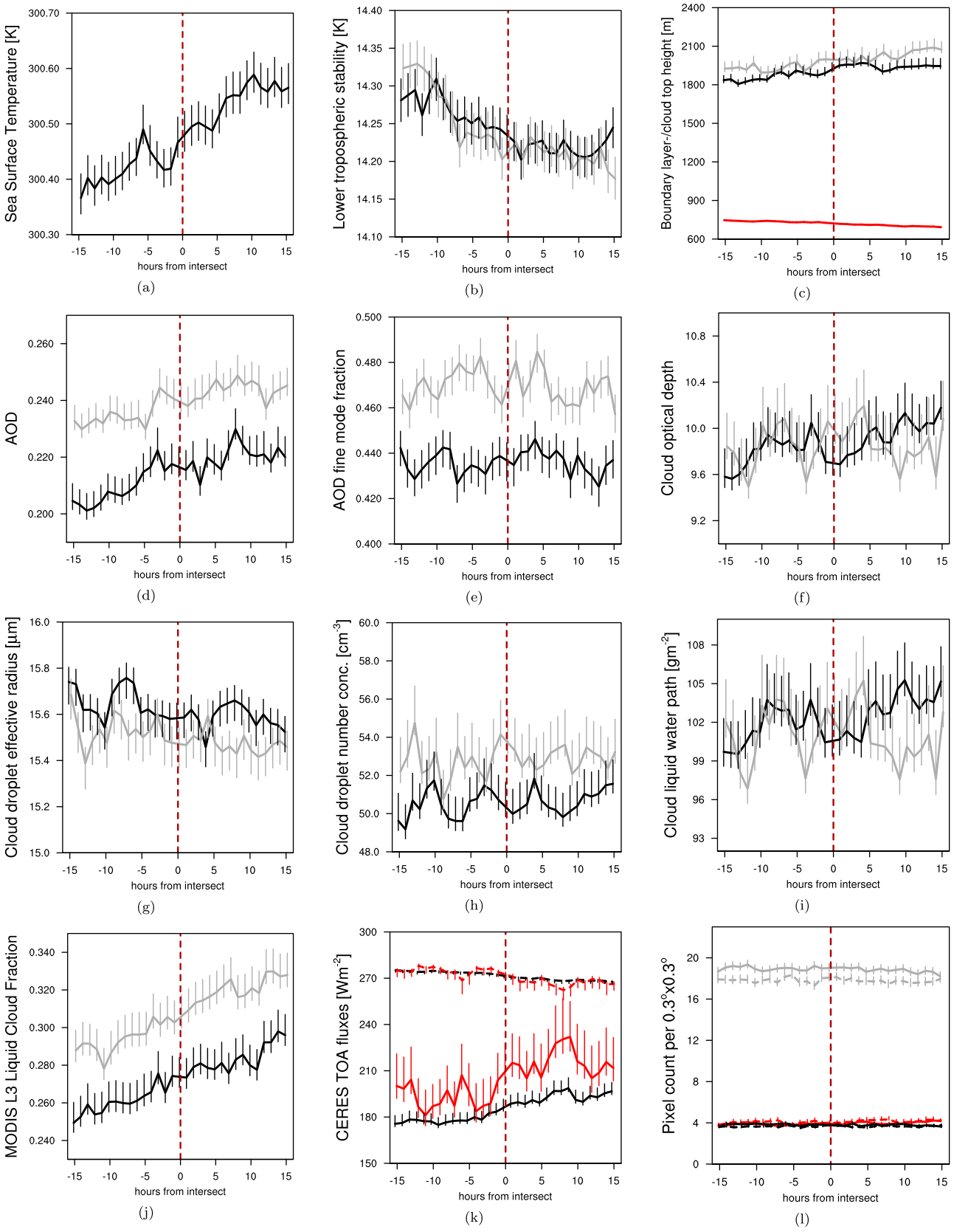

Figure 8. Same as Figure 7 but for the mid-Atlantic region.

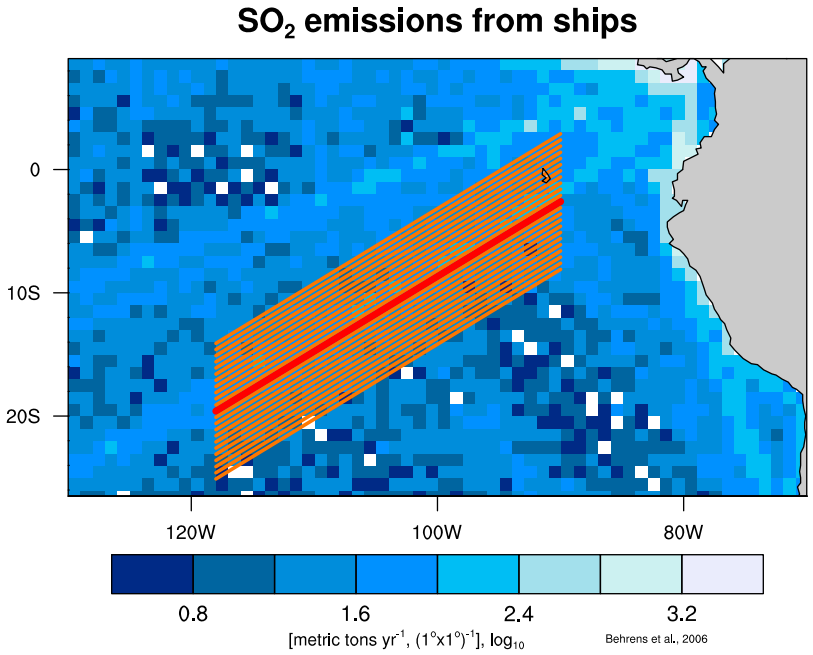

Figure 9. Illustration of the Eulerian analysis concept demonstrated for the shipping lane in the southeast Pacific Ocean region. The thick red line is the shipping lane. Cloud and aerosol properties for the "clean" and "polluted" regions are sampled along the thin lines to the south and the north of the shipping lane, respectively.

lane. The shift between each straight line is 0.5° and there are eleven of these straight lines upwind and downwind of the shipping lane, i.e., we are sampling the region 5.5° upwind and downwind of the shipping lane. The concept is illustrated in Figure 9. We hypothesize that the mean MBL composition in the area downwind of the shipping lane is more polluted from shipping emissions than the area upwind. Therefore, the retrieved cloud and aerosol properties should be different in such a way that their change in across-corridor direction can be associated with the shipping emissions at the position of the shipping lane. The sampling is done only for days where the 10 m wind obtained from the ERA-Interim Reanalysis blows in the predominant direction, to assure that the definition of upwind and downwind remains consistent.

[41] We collect the geophysical data of interest along these straight lines in such a way that the data fall into squares of edge length 0.3°. The squares have their centers lying on the lines so that they extend 0.15° on either side of the line (see Figure 10). The edge length of 0.3° is chosen to ensure that there is no data overlap between two neighboring lines. We compute the average of all measurements falling into each square. Because we sample on a daily basis, we can assume the local meteorology as being roughly similar in the region of interest.

[42] The main advantage of this Eulerian perspective over the previous Lagrangian one is that a much larger amount of data can be investigated. The aim here is to average over even more situations to potentially average out "noise" due to the natural variability in the large-scale meteorology, which was found to mainly drive the variability in the boundary layer clouds. Thus, we do not necessarily expect to obtain identical results for both approaches. For the Lagrangian approach, we only sample along a uniquely defined wind trajectory and exclude all other data from a particular day. By this, the data is strictly filtered prior to the final analysis. For the Eulerian approach, on the other hand, all data from the shipping corridor are analyzed on a daily basis. By this, the data are less filtered compared to the Lagrangian approach, a much larger area is covered and the spectrum of possible observed situations is broader. This may give differences in the observed aerosol and cloud properties. The method for deriving the mean values and respective error estimates is the same as that described for the Lagrangian approach (see section 4.1).

5.2. Results

5.2.1. Southeast Pacific Ocean

[43] For the southeast Pacific region, we perform the analysis for that part of the shipping lane which extends from 118°W to 100°W. We exclude any data eastward of 100°W because there the environmental conditions do not

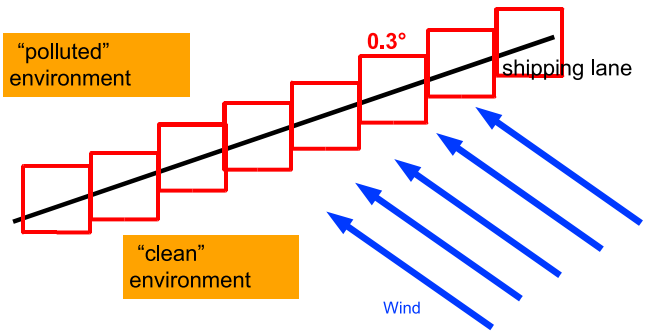

Figure 10. Conceptual illustration of the Eulerian analysis concept (not to scale).

guarantee similar conditions with respect to the more westward part of the shipping lane. The SST gradient, in particular, shows varying patterns: SST first increases in the clean part and then decreases in the polluted part. For the region spanning 118°W–100°W, SST continuously increases in across-corridor direction. Additionally, the retrieved cloud properties eastward of about 95°W are influenced by the Galapagos Islands (different MODIS algorithm for land surfaces), and most satellite pixels do not pass our filtering for ice and multilevel clouds eastward of about 85°W, which is probably associated with deep convection in close proximity to the ITCZ. Furthermore, data taken eastward of 90°W would be too close to continental South America.

[44] It is mostly because of this spatial restriction that we obtain different characteristics of the observed aerosol and cloud distributions compared to the Lagrangian approach shown in section 4.2.1. In the Lagrangian approach, most of the trajectories cluster in the longitudinal band of 90°W–105°W. Furthermore, as the averaging direction of the Lagrangian approach was rather zonal (wind directions ≈100°–120°), the results from the Eulerian analysis reflect the zonally averaged meridional gradient across the shipping corridor. Therefore, there is little overlap among the two analysis approaches in both the sampled region and averaging procedure. This then leads to different statistical results among the two methods. Nevertheless, the main conclusions remain untouched by this.

[45] We show the 3 year across-corridor average values of selected meteorological parameters and cloud properties as a function of distance to the shipping lane in Figure 11.

[46] For the corridor extending from 118°W to 100°W, we find an annually persistent increase in SST from the clean to the polluted area. We find the LTS to have a maximum close to the shipping lane with the values on the clean and polluted sides being lower by ≈0.5 K. The BLH as obtained from the reanalysis is approximately constant throughout the clean side of the corridor and then decreases by about 10% on the polluted side. The BLH proxy values suggest (1) a constant decrease in BLH in across-corridor direction and (2) a much deeper boundary layer than the BLH values obtained from the reanalysis. So as for the Lagrangian approach, the LTS does not follow the general increase in SSTs which would suggest a destabilization of the lower troposphere.

[47] Unlike the Lagrangian approach, the number of valid cloudy pixels available for analysis per 0.3° × 0.3° box increases in across-corridor direction; but the ratio of valid versus invalid pixels is nevertheless small. Similar to the Lagrangian approach, we find the AOD to systematically increase by about 20% from the clean to polluted side of the sampled region, and AODs retrieved from MODIS (Terra) are also higher than those from MODIS (Aqua). The FMF associated with the AOD is on the order of the oceanic background value [*Remer et al.*, 2008] and slightly increases toward the polluted side of the shipping corridor. Whether or not this relative increase in small-particle extinction in across-corridor direction can be associated with shipping emissions is not clear; it is also present in the results from the Lagrangian analysis, though. Similar to the results found for the Lagrangian approach, the systematic increase in total AOD cannot be linked to shipping emissions because we do not find a substantial increase of AOD or its associated FMF in the vicinity of the shipping lane. Therefore, we also do not detect an aerosol DRE from the Eulerian approach.

[48] The calculated CDNC substantially increases in across-corridor direction with the values obtained from MODIS (Terra) (≈40%) being slightly higher than those from Aqua (≈36%). The LWP shows different patterns in across-corridor directions for the two instruments: while the LWP continuously decreases for data from Terra, it first decreases and then increases for Aqua; these changes in LWP are within a range of 5% though and may be attributed to the diurnal cycle of shallow convection. The same holds for the liquid cloud fraction as obtained from the MODIS Level 3 product. Compared to the results from the Lagrangian analysis, the gradients in retrieved cloud properties between the clean and polluted sides of the shipping corridors are much larger here.

[49] From the trends in the aerosol and cloud properties, we could claim to have isolated an aerosol indirect effect for this region. To further corroborate our analysis, we also investigate the changes in CTH of the sampled cloud fields because an increase in CTH and LWP could indicate an AIE [e.g., *Koren et al.*, 2005]. In such a case, the retrieved r_{eff} at cloud top should stay approximately unchanged compared to an unpolluted cloud because r_{eff} at cloud base is smaller and generally increases with height. On the other hand if CTH and r_{eff} decrease, and LWP stays constant or increases, AIEs could also explain this relationship because (1) the vertical extent of the cloud remains approximately unchanged which implies that (2) the r_{eff} profile is shifted toward smaller sizes. The MODIS-retrieved CTP values (not shown) show a pattern consistent with the BLH: they are relatively constant on the clean side and then increase on the polluted side of the corridor. Therefore, the change in CTH as deduced from MODIS data is most probably due to dynamical drivers associated with the decrease in BLH [e.g., *Wood and Bretherton*, 2004] as retrieved from the ERA-Interim reanalyses.

[50] Recently, it has been investigated that MODIS-retrieved CTP values suffer from severe underestimation (i.e., CTH overestimation) under specific meteorological conditions [*Ludewig*, 2011]. Therefore, we also check for CTH as retrieved from MISR and CALIPSO measurements and find similar across-corridor patterns for the three instruments (MISR CTH in Figure 12, CALIPSO CTH not shown); MISR and CALIPSO CTHs show very good agreement. As CALIPSO-retrieved CTH is often used as a reference, we conclude that the CTH gradient retrieved from MODIS is a robust result.

[51] Overall, the analyzed data suggest a first indirect aerosol effect: an increase in AOD and associated FMF is accompanied by increased CDNC and almost constant LWP. Furthermore, to maintain the approximately constant or even increasing LWP values in across-corridor direction with decreasing CTH, the cloud base height should decrease as well. because the vertical extent of the clouds should remain about the same. Then, the decrease in MODIS-retrieved r_{eff} can only be explained by an overall shift of the r_{eff} profile toward smaller sizes. There is, on the other hand, no evidence at all for a cloud lifetime effect (cloud fraction decreases rather than increases), and also CTHs decrease rather than increase. Most importantly, no discernible effect

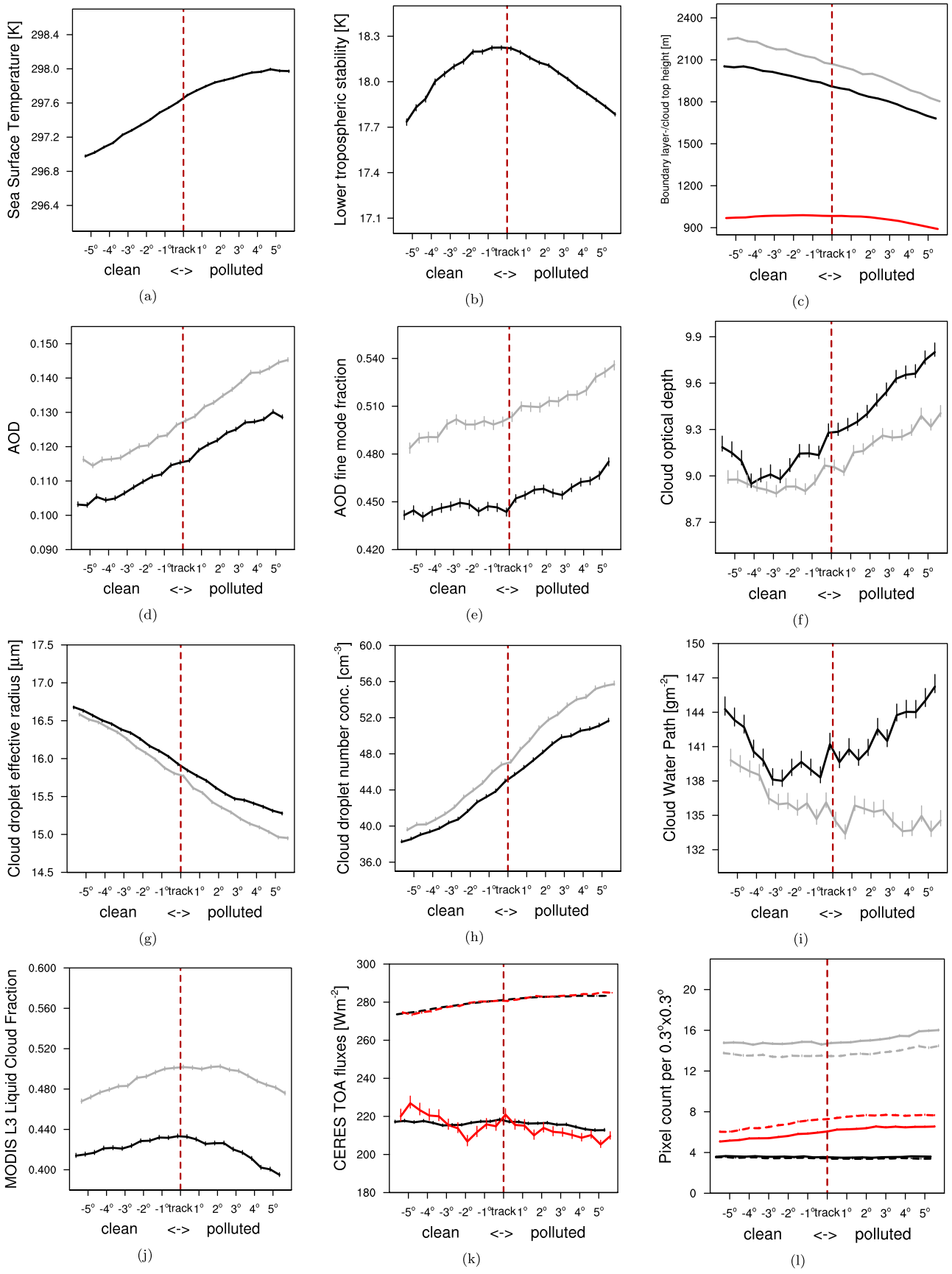

Figure 11. Same as Figure 7 but applying the Eulerian sampling method.

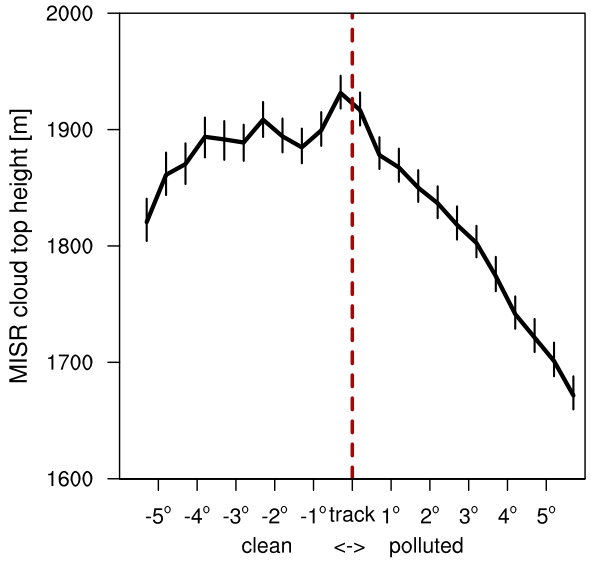

Figure 12. Cloud top heights of low (liquid water) clouds as retrieved from the MISR aboard Terra for the southeast Pacific region. Data are from the months September–November of 2005–2007. The error bars denote the confidence in the calculated mean value toward higher/lower values (see section 3).

is visible in the radiation; the dominant influence on it is the change in cloud fraction, opposite to the expected aerosol indirect forcing.

5.2.2. Mid-Atlantic Ocean

[52] Just as for the analysis of the southeast Pacific region, we do not sample data along the whole latitudinal extent of the shipping lane. We exclude data southward of 5S because of possible "landmass contamination" and northward of 2 N because of an increasing number of observations being filtered out due to ice cloud presence. For the Lagrangian approach (see section 4.2.2), most trajectories cluster in the latitudinal range of 3°S–3°N. Therefore, the sampled region discussed here is shifted slightly southward compared to the Lagrangian approach and the results of the analysis are shown in Figure 13.

[53] Similar to the results obtained from the Lagrangian analysis, we find the SST to increase by about 0.5 K from the clean to the polluted side of the corridor. This across-corridor SST gradient is subject to interseasonal variability within the uncertainty range given. The LTS as obtained from the reanalysis data decreases from ≈15 K to ≈14 K and the BLH as obtained from the reanalysis correspondingly slightly increases in across-corridor direction. Our calculated BLH proxy values again indicate a distinctly deeper boundary layer and the across-corridor increase in BLH is also more pronounced than in the reanalysis data. Interestingly, this is partly in contradiction to the results from the Lagrangian approach: there, the LTS also decreases, much less though (≈0.1 K), but the BLH slightly increases (≈20 m).

[54] The observed gradients in across-corridor direction are similar for both MODIS sensors and as for the Lagrangian approach, the number of valid pixels is about the same for both cloud and aerosol retrievals. The AOD decreases over the whole shipping corridor by about 10% (Lagrangian approach: increasing AOD), with the AOD retrieved from MODIS (Terra) showing the previously mentioned offset to MODIS (Aqua). Therefore, there is no aerosol DRE from shipping emissions detectable in this region also. We find the AOD FMF to be almost constant in across-corridor direction at approximately the oceanic background value as shown by *Remer et al.* [2008]. This is particularly interesting because our ship emissions inventory shows the highest shipping emissions of the three corridors under investigation for the region of the mid Atlantic Ocean (Figure 2).

[55] The liquid cloud fraction as retrieved from the aggregated MODIS Level 3 product shows a constant decrease across the shipping corridor with values around 0.3 indicating rather broken trade cumulus cloud fields. This is the same order of magnitude as found with the Lagrangian approach; there, the cloud fraction increases though. We find the r_{eff} to increase by about 10% which also holds for τ. Our calculations of the CDNC show a significant decrease (≈23%–33%) in across-corridor direction and the LWP increases across the whole corridor (Lagrangian approach: CDNC and LWP about constant). This is accompanied by an increase in CTH.

[56] The results obtained from this analysis approach indicate that we are just sampling a change in mean cloud properties associated with the across-corridor increase in SST [e.g., *Betts and Ridgway*, 1989] The important measure in this regard is the change in CTH across the shipping corridor. All other results follow from this: assuming no change in cloud base height, the increase in CTH leads to increased cloud geometrical thickness, LWP and τ. Keeping the adiabatic r_{eff} profile in mind, we deduce that the increase in the retrieved r_{eff} is associated with the increased cloud geometrical thickness. The results for CERES TOA radiative fluxes also support this finding: the shortwave flux increases and the longwave flux decreases along the mean trajectory. Clouds get more reflective along the trajectories sampled, which explains the increased shortwave fluxes. The clouds also have higher cloud tops with lower cloud temperatures, which explains the along-trajectory reduction of the outgoing TOA longwave fluxes. Therefore, we do not find that the observed across-corridor change in cloud properties is to be associated with shipping emissions. The observed gradient can be solely explained by the observed meteorological conditions of this region. This is also in line with our finding that the AOD decreases and that the FMF stays about constant in across-corridor direction. Because one would expect a somewhat pronounced signal in the AOD and its FMF due to the across-track gradient in shipping emissions (see Figure 2), these results shed light on the difficulties of determining aerosol indirect effects in dynamically active cloud regimes.

[57] Interestingly, the results obtained for this region differ greatly between the two statistical analysis approaches. For the Eulerian approach discussed in this section, we do not apply such stringent dynamical constraints as for the Lagrangian approach, e.g., such as that a "useful" trajectory must not exceed a height of 500 m above sea level which by common sense excludes highly convective environments. Therefore, it is possible that we sample distinctly different lower tropospheric conditions between the two approaches.

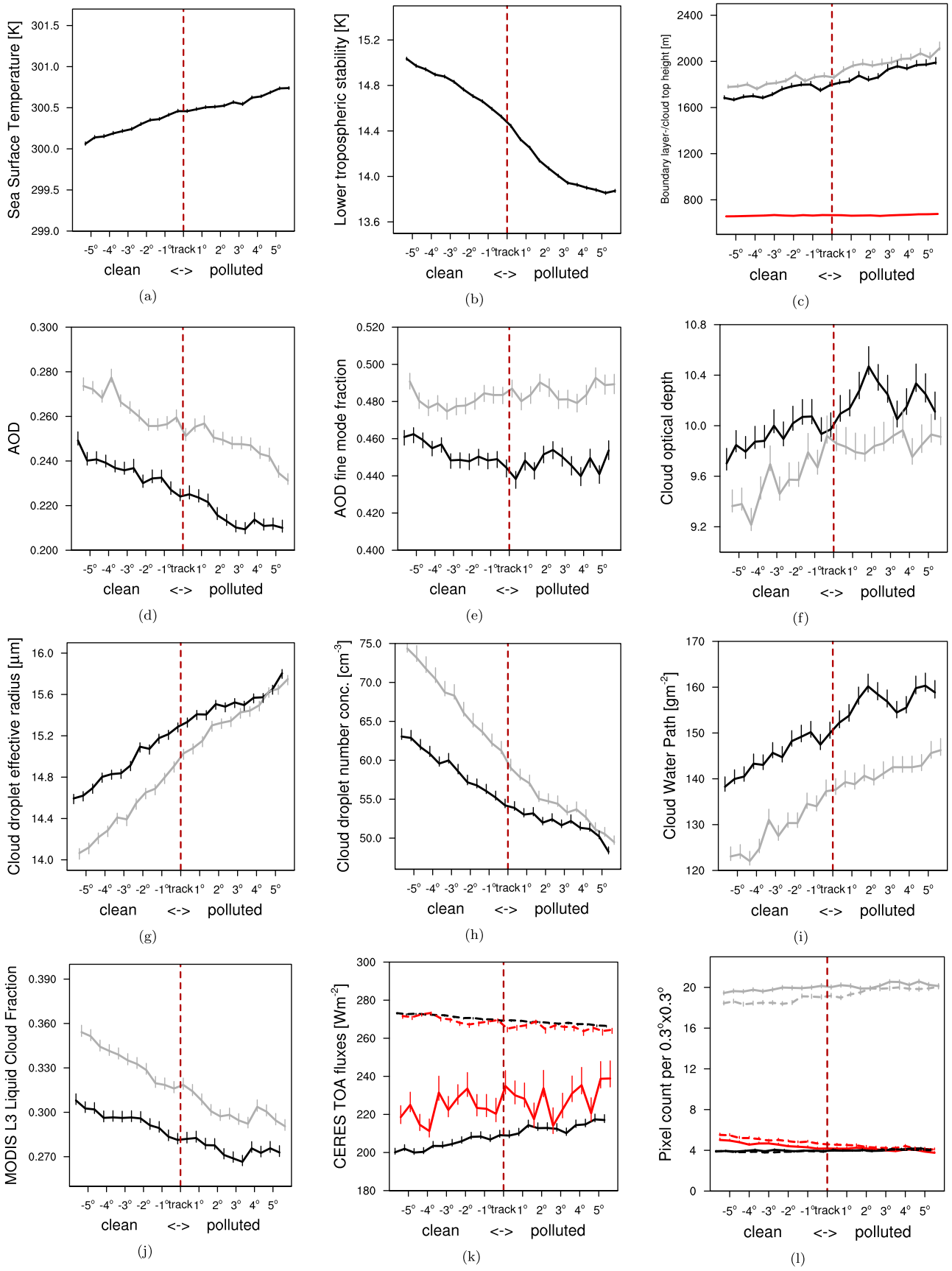

Figure 13. Same as Figure 8 but applying the Eulerian sampling method.

5.2.3. Mid-Indian Ocean

[58] For the shipping corridor in the mid Indian Ocean, we only use data in the range from 56°E to 75°E because (1) data westward of 60°E would be influenced by Madagascar and Mauritius and (2) the across-corridor mean cloud properties eastward of 75°E are significantly different from those in the rest of the corridor. Furthermore, we exclude data from the northern hemispheric winter season (DJF) as the mean wind direction in across-corridor direction in this season differs distinctly from that obtained for the other seasons. This is due to the circulation patterns associated with the Indian winter monsoon. As for the other two regions, we show 3 year mean values of selected meteorological quantities as well as cloud and aerosol properties as a function of distance from the shipping lane in the mid Indian Ocean in Figure 14.

[59] Similar to the other two shipping corridors under investigation, we find an annually persistent increase of the SST across the corridor of almost 2 K, which is the largest change in across-corridor SST amongst the three analyzed shipping corridors. The LTS decreases by about 0.7 K and the BLH also decreases by more than 200 m. As for the other two regions, the BLH proxy values suggest a substantially deeper MBL than that obtained from the reanalysis. Furthermore, the proxy values suggest a rather constant BLH whereas the reanalysis data suggest a constant decrease in across-corridor direction.

[60] For this corridor, the results are mostly consistent among the two MODIS sensors if not mentioned otherwise. The number of pixels per 0.3° × 0.3° box available for analysis of cloud properties slightly decreases in across-corridor direction and converges to the number of available aerosol retrievals. Near the location of the shipping lane, both the AOD and its FMF show a change in across-corridor gradient: the AOD peaks or levels off and the FMF increases from thereon. These gradients are similar for both data sets which gives confidence in this result and implies no aerosol DRE from shipping emission in this region also.

[61] The gradient in CDNC values shows decreasing values (≈−(12%–17%)) in the clean part followed by a leveling off or even a slight increase in the polluted part of the shipping corridor. The analysis of the retrieved τ and derived LWP reveals the largest differences between the two instruments: τ and LWP as retrieved from MODIS (Aqua) stay about constant or increase in across-corridor direction whereas the same parameters retrieved from MODIS (Terra) measurements rather decrease on the clean side and then stay approximately constant on the polluted side. The liquid cloud fraction decreases by about 10% in across-corridor direction with the largest part of this reduction occurring on the polluted side of the corridor.

[62] The most interesting analyzed quantity for this region is the FMF of the observed AOD, with a distinct but not large increase from the position of the shipping lane into the polluted side of the shipping corridor. Here, it is tempting to say that we have indeed sampled scenes in which the size distribution of the aerosol population has changed due to shipping emissions. Nevertheless, it remains an open question, why the retrieved AOD increases throughout the clean side of the shipping corridor and then levels off on the polluted side. The across-corridor gradients of the calculated CDNC also show a distinct change near the point of the shipping lane: the profiles level off. Therefore, CDNC correlates negatively with the retrieved AOD whereas a positive correlation would generally be expected when considering the "Twomey effect." Nevertheless, this negative correlation could very well be the background conditions of this region and shipping emissions at the shipping lane disturb these conditions. From this perspective, the relative increase in small particle numbers then leads to altered cloud properties, because had the gradients from the clean region persisted into the polluted region, the cloud droplet radii would have been considerably larger and CDNC considerably smaller than observed. Likewise, τ as retrieved from Terra observations would have been considerably smaller. Interestingly, the all-sky TOA shortwave radiative fluxes show an increase larger than the mean gradient near the point of the shipping lane.

[63] So overall, our analysis of the mid Indian Ocean shipping corridor reveals apparent correlations between observed aerosol and cloud properties. These could be indicative of a first indirect effect from shipping emissions but dynamical drivers cannot be ruled out: the across-corridor increase in SST is the largest among the three analyzed regions. From this point of view, it is interesting that we do not find a more significant change in cloud macrophysical properties because a distinct increase in CTH should be observed from the observed 2 K increase in SST [e.g., *Betts and Ridgway*, 1989].

6. Summary and Conclusions

[64] To investigate the influence of shipping emissions on climatically relevant scales, we used satellite and reanalysis data to sample parameters characterizing the cloud, aerosol, and radiative properties as well as the large-scale meteorological conditions of several remote oceanic regions. These remote oceanic regions were selected according to the following criteria: (1) a well-defined shipping lane leading through an otherwise pristine environment is present, (2) the mean low-level wind directions are not too close to being parallel with this shipping lane, and (3) the so-defined shipping corridor is not subject to significant pollution advected from a nearby landmass. This definition fits three shipping corridors which we then selected for our analysis: (1) the southeast Pacific Ocean with the shipping lane from the Panama Canal southwestward, (2) the mid Atlantic Ocean with the shipping lane from Europe to South America, and (3) the mid Indian Ocean with the shipping lane from Madagascar to Indonesia.

[65] In short, our statistical analysis, following an either Lagrangian or Eulerian approach, did not reveal sound evidence of ship emission influence on the microphysical and macrophysical properties of the large-scale cloud fields that we analyzed in this study. More specifically, gradients in aerosol optical depth, its fine-mode fraction, and in cloud droplet number concentration are consistent with an, albeit relatively small, Twomey effect due to ship emissions in two out of the three regions (except in the mid Atlantic, where no discernible effect on aerosol concentrations is found). However, cloud properties that are more relevant to the radiation budget (cloud fraction, cloud liquid water path and cloud top temperature) change across the ship tracks in various ways, which may be better explained by gradients in the large-scale

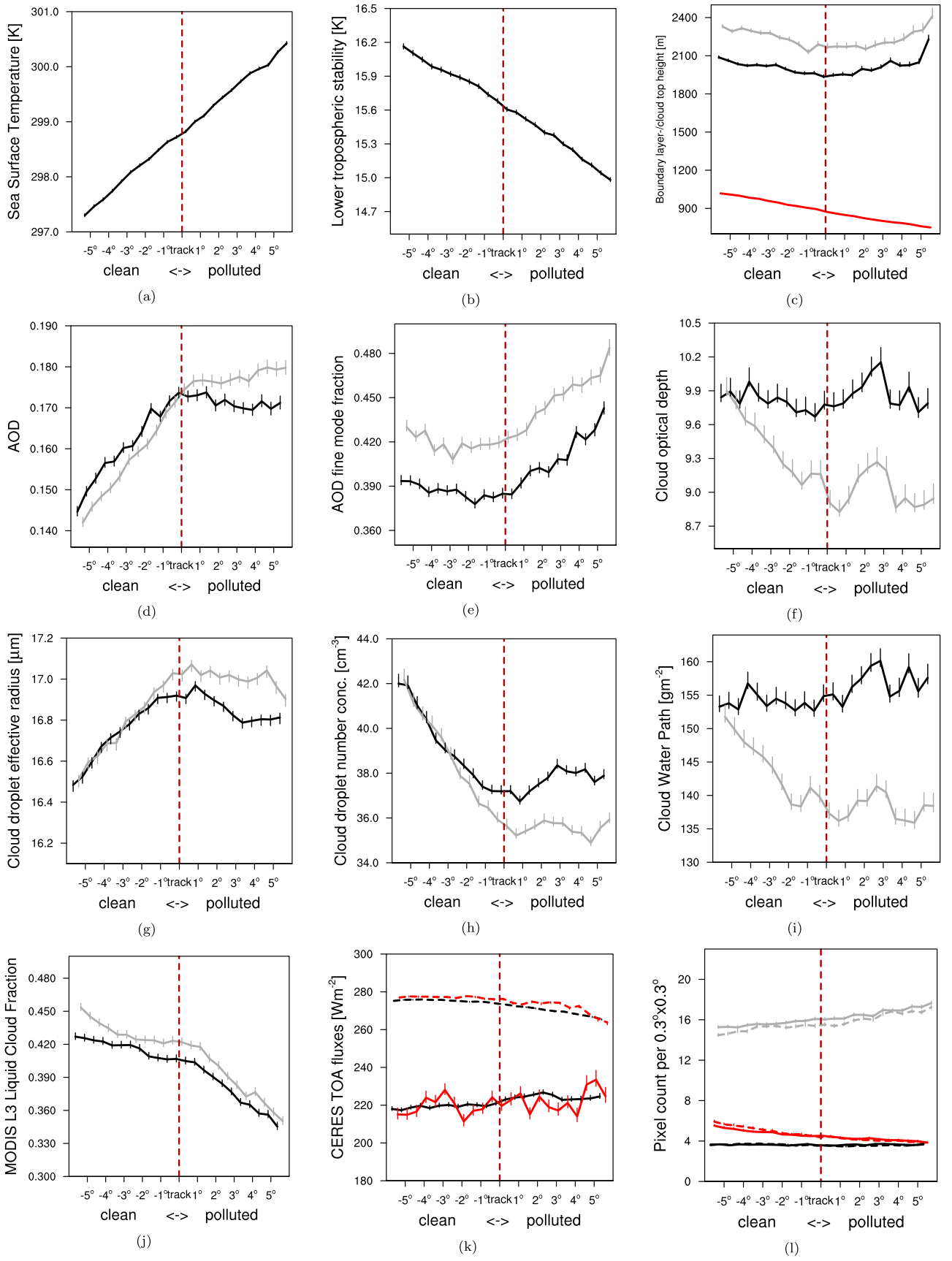

Figure 14. Same as Figures 11 and 13 but for the mid Indian Ocean region.

meteorology than by any single concept of secondary aerosol indirect effects. In particular in the Indian Ocean region, which is close to the ITCZ, convective dynamics may have such a large influence on the cloud fields that the signal-to-noise ratio stemming from any microphysical perturbations due to ship emissions is very small. Thus, no effect of the ship emissions on the radiation budget is discernible, and in conclusion, no discernible aerosol indirect effect of ship emissions can be identified. However, we must again stress that the results found in this study only apply to the regions investigated here. Cloud systems in other regions, e.g., regions characterized by persistent stratocumulus fields, are known for their susceptibility with respect to shipping emissions. Furthermore, we did not investigate those regions with the most intense ship traffic, such as the northern Atlantic or northern Pacific oceans due to limitations of the available data.

[66] We found gradients suggesting ship emission influence in the retrieved AOD and its fine-mode fraction (FMF) in the SE Pacific and mid Indian Ocean regions. In these two corridors, the FMF increases from the clean to the polluted sides of the shipping corridor which suggests a larger fraction of small particles downwind of the shipping lane. It is also in these two regions where the retrieved cloud properties indicate a possible first AIE: for the shipping corridor in the southeast Pacific Ocean we found the expected positive correlation of the AOD with CDNC. In the mid Indian Ocean region, we find a change in the across-corridor gradients of the retrieved cloud properties near the point of the shipping lane, e.g., the systematic decrease in CDNC in the clean side does not continue into the polluted side of the corridor. So from the retrieved cloud droplet number concentration and aerosol parameters, we find effects consistent with a Twomey aerosol indirect effect in these two out of three regions. However, the across-corridor gradients of total AOD do not support a possible aerosol direct radiative effect (DRE) in any of the three regions. As model estimates of the aerosol DRE from shipping are small and range from -47.5 to -9.1 m Wm^{-2} [*Eyring et al.*, 2010, and references therein], its detection in satellite data for the regions we investigated in our study seems highly unlikely.

[67] In the mid Atlantic Ocean on the other hand, the obtained across-corridor gradients of aerosol properties do not yield such a clear picture. For the Lagrangian approach, the AOD increases from the clean to the polluted side of the trajectories whereas the opposite is true for the Eulerian analysis. These differences are probably due to differences in the filtering for analyzed scenes (see section 5.2.2).

[68] To characterize the local meteorology, we sampled, among other parameters, the SST as retrieved from microwave remote sensing and found increasing values from the clean to the polluted sides of the corridors for all three corridors. This is of particular interest, because a large number of modeling studies have found a positive correlation between SST and CTH [see, e.g., *Betts and Ridgway*, 1989]. The retrieved CTHs did not show this relationship with SST in all corridors: in the southeast Pacific region, the increase in SST is accompanied by a decrease in CTH, whereas the CTH mostly increased with increasing SST for the other two regions of interest.

[69] In a recent modeling effort, *Lauer et al.* [2007] estimated that emissions from shipping may lead to a significant negative TOA radiative forcing due to aerosol indirect effects of up to -0.6 Wm^{-2} when implemented into a general circulation model (GCM) with interactive aerosol representation. They show the zonal mean increase in CDNC due to shipping emissions over Southern Hemisphere tropical oceans to be on the order of 2–12 cm^{-3} which suggests this increase being substantially larger in regions of intense shipping. In our Lagrangian analysis, we obtained along-trajectory gradients in CDNC of $\approx$2 cm^{-3} for both regions. From the Eulerian analysis, we obtain constant across-corridor gradients leading to differences in the range 10–25 cm^{-3} for the mid Atlantic and southeast Pacific Ocean regions. Thus, in the mid Atlantic and southeast Pacific Ocean regions, our analysis does not reveal a change in CDNC as a result from shipping emissions as suggested by the estimates of *Lauer et al.* [2007]. But in the mid Indian Ocean, our results are somewhat consistent with the modeling estimates. There, CDNC shows an apparent decrease across the clean part of the shipping corridor. Near the shipping lane, the gradient levels off and CDNC stays constant or even increases throughout the polluted part. If this change in across-corridor gradient is due to shipping emissions and CDNC were to further decrease under undisturbed conditions, the shipping emissions lead to an increase in CDNC by 4–6 cm^{-3} in the polluted part. This value would meet the lower end of the estimates by *Lauer et al.* [2007].

[70] With shipping traffic bound to increase in the next decades, it remains a challenging task to quantify its emissions' effects on the TOA radiation budget from measurements. However, the uncertainties associated with satellite sensor retrieval algorithms and their inability to deliver sound results for multilayered cloud systems hampers their usability in regions with the highest shipping emissions, i.e., in the northern midlatitudes. With the technical possibilities available today, the approach that we took in this study therefore may represent the best possible one to tackle possible aerosol indirect effects from shipping emissions on large-scale environments other than regions governed by stratocumulus clouds.

[71] **Acknowledgments.** The authors would like to thank the three reviewers whose comments helped to significantly improve the manuscript, Axel Andersson for helpful input on an earlier version of the paper, Bjorn Stevens for the initial idea of the analysis approach, and Irina Sandu for assistance with the Lagrangian trajectories. CERES SSF data were obtained from the NASA Langley Research Center Atmospheric Sciences Data Center. MODIS data used in this study were acquired as part of NASA's Earth Science Enterprise. The MODIS science teams developed the algorithms for the AOD retrievals. The data were processed by the MODIS Adaptive Processing System and the Goddard Distributed Active Archive (DAAC). AMSR-E data are produced by Remote Sensing Systems and sponsored by the NASA Earth Science REASoN DISCOVER Project and the AMSR-E science team. Data are available at www.remss.com. This work was partly funded by the European Union FP6 Integrated Project QUANTIFY and by the European Commission under the EU Seventh Research Framework Programme (grant 218793, MACC).

References

Albrecht, B. A. (1989), Aerosols, cloud microphysics, and fractional cloudiness, *Science*, *245*, 1227–1230.

Ångström, A. (1962), Atmospheric turbidity, global illumination and planetary albedo of the Earth, *Tellus*, *14*(4), 435–450.

Bellouin, N., A. Jones, J. Haywood, and S. A. Christopher (2008), Updated estimate of aerosol direct radiative forcing from satellite observations and comparison against the Hadley Centre climate model, *J. Geophys. Res.*, *113*, D10205, doi:10.1029/2007JD009385.

Betts, A. K., and W. Ridgway (1989), Climatic equilibrium of the atmospheric convective boundary layer over a tropical ocean, *J. Atmos. Sci.*, *46*, 2621–2641.

Campmany, E., R. G. Grainger, S. Dean, and A. M. Sayer (2009), Automatic detection of ship tracks in ATSR-2 satellite imagery, *Atmos. Chem. Phys.*, *9*, 1899–1905, doi:10.5194/acp-9-1899-2009.

Capaldo, K., J. Corbett, P. Kasibhatla, P. Fischbeck, and S. Pandis (1999), Effects of ship emissions on sulphur cycling and radiative climate forcing over the ocean, *Nature*, *400*, 743–746.

Christensen, M. W., and G. L. Stephens (2011), Microphysical and macrophysical responses of marine stratocumulus polluted by underlying ships: Evidence of cloud deepening, *J. Geophys. Res.*, *116*, D03201, doi:10.1029/2010JD014638.

Christensen, M. W., J. A. Coakley Jr., and W. E. Tahnk (2009), Morning-to-afternoon evolution of marine stratus polluted by underlying ships: Implications for the relative lifetimes of polluted and unpolluted clouds, *J. Atmos. Sci.*, *66*, 2097–2106, doi:10.1175/2009JAS2951.1.

Coakley, J. A., and C. D. Walsh (2002), Limits to the aerosol indirect radiative effect derived from observations of ship tracks, *J. Atmos. Sci.*, *59*, 668–680.

Coakley, J. A., R. J. Bernstein, and P. A. Durkee (1987), Effect of ship-stack effluents on cloud reflectivity, *Science*, *237*(4818), 1020–1022.

Conover, J. H. (1966), Anomalous cloud lines, *J. Atmos. Sci.*, *23*, 778–785.

Dalsøren, S. B., M. S. Eide, Ø. Endresen, A. Mjelde, G. Gravir, and I. S. A. Isaksen (2009), Update on emissions and environmental impacts from the international fleet of ships: The contribution from major ship types and ports, *Atmos. Chem. Phys.*, *9*, 2171–2194, doi:10.5194/acp-9-2171-2009.

Devasthale, A., O. Krüger, and H. Grassl (2005), Change in cloud-top temperatures over Europe, *IEEE Geosci. Remote S.*, *2*(3), 333–336, doi:10.1109/LGRS.2005.851736.

Devasthale, A., O. Krüger, and H. Grassl (2006), Impact of ship emissions on cloud properties over coastal areas, *Geophys. Res. Lett.*, *33*, L02811, doi:10.1029/2005GL024470.

Durkee, P., K. Noone, and R. Bluth (2000), The Monterey area ship track experiment, *J. Atmos. Sci.*, *57*, 2523–2541.

Dusek, U., et al. (2006), Size matters more than chemistry for cloud-nucleating ability of aerosol particles, *Science*, *312*(5778), 1375–1378, doi:10.1126/science.1125261.

Endresen, Ø., E. Sørgård, J. K. Sundet, S. Dalsøren, I. S. A. Isaksen, T. F. Berglen, and G. Gravir (2003), Emission from international sea transportation and environmental impact, *J. Geophys. Res.*, *108*(D17), 4560, doi:10.1029/2002JD002898.

Eyring, V., H. W. Köhler, J. van Aardenne, and A. Lauer (2005), Emissions from international shipping: 1. The last 50 years, *J. Geophys. Res.*, *110*, D17305, doi:10.1029/2004JD005619.

Eyring, V., et al. (2010), Transport impacts on atmosphere and climate: Shipping, *Atmos. Environ.*, *44*(37), 4735–4771, doi:10.1016/j.atmosenv.2009.04.059.

Forster, P., et al. (2007), Changes in atmospheric constituents and in radiative forcing, in *Climate Change 2007: The Physical Science Basis, Contribution of Working Group I to the Fourth Assessment Report of the Intergovernmental Panel on Climate Change*, edited by S. Solomon et al., pp. 129–234, Cambridge Univ. Press, Cambridge, U. K.

Hayes, C. R., J. A. Coakley Jr., and W. R. Tahnk (2010), Relationships among properties of marine stratocumulus derived from collocated CALIPSO and MODIS observations, *J. Geophys. Res.*, *115*, D00H17, doi:10.1029/2009JD012046.

Haywood, J., and O. Boucher (2000), Estimates of the direct and indirect radiative forcing due to tropospheric aerosols: A review, *Rev. Geophys.*, *38*(4), 513–543, doi:10.1029/1999RG000078.

Hewson, E. (1943), The reflection, absorption, and transmission of solar radiation by fog and cloud, *Q. J. R. Meteorol. Soc.*, *69*(301), 227–234.

Hobbs, P., et al. (2000), Emissions from ships with respect to their effects on clouds, *J. Atmos. Sci.*, *57*, 2570–2590.

Houze, R. A. (1994), *Cloud Dynamics*, *Int. Geophys.*, vol. 53, Academic, San Diego, Calif.

International Maritime Organization (1998), Regulations for the prevention of air pollution from ships and NO_x technical code, Annex IV, MARPOL 73/78, technical report, London.

Klein, S. A., and D. L. Hartmann (1993), The seasonal cycle of low stratiform clouds, *J. Clim.*, *6*(8), 1587–1606.

Koren, I., Y. J. Kaufman, D. Rosenfeld, L. A. Remer, and Y. Rudich (2005), Aerosol invigoration and restructuring of Atlantic convective clouds, *Geophys. Res. Lett.*, *32*, L14828, doi:10.1029/2005GL023187.

Kotarba, A. Z. (2010), Estimation of fractional cloud cover for Moderate Resolution Imaging Spectroradiometer/Terra cloud mask classes with high-resolution over ocean ASTER observations, *J. Geophys. Res.*, *115*, D22210, doi:10.1029/2009JD013520.

Langley, L., W. R. Leaitch, U. Lohmann, N. C. Shantz, and D. R. Worsnop (2010), Contributions from DMS and ship emissions to CCN observed over the summertime North Pacific, *Atmos. Chem. Phys.*, *10*, 1287–1314.

Lauer, A., V. Eyring, J. Hendricks, P. Jöckel, and U. Lohmann (2007), Global model simulations of the impact of ocean-going ships on aerosols, clouds, and the radiation budget, *Atmos. Chem. Phys.*, *7*, 5061–5079.

Lauer, A., V. Eyring, J. J. Corbett, C. Wang, and J. J. Winebrake (2009), Assessment of near-future policy instruments for oceangoing shipping: Impact on atmospheric aerosol burdens and the Earth's radiation budget, *Environ. Sci. Technol.*, *43*(15), 5592–5598, doi:10.1021/es900922h.

Loeb, N. G., and N. Manalo-Smith (2005), Top-of-atmosphere direct radiative effect of aerosols over global oceans from merged CERES and MODIS observations, *J. Clim.*, *18*(17), 3506–3526, doi:10.1175/JCLI3504.1.

Lu, M.-L., W. C. Conant, H. H. Jonsson, V. Varutbangkul, R. C. Flagan, and J. H. Seinfeld (2007), The Marine Stratus/Stratocumulus Experiment (MASE): Aerosol-cloud relationships in marine stratocumulus, *J. Geophys. Res.*, *112*, D10209, doi:10.1029/2006JD007985.

Ludewig, E. (2011), Evaluation of satellite cloud-top height measurements along stratocumulus to cumulus transition trajectories, diploma thesis, 128 pp., Meteorol. Inst., Univ. Hamburg, Hamburg, Germany.

Marbach, T., et al. (2009), Satellite measurements of formaldehyde linked to shipping emissions, *Atmos. Chem. Phys.*, *9*, 8223–8234, doi:10.5194/acp-9-8223-2009.

McCormick, R. A., and J. H. Ludwig (1967), Climate modification by atmospheric aerosols, *Science*, *156*(3780), 1358–1359.

Nakajima, T., and M. King (1990), Determination of the optical thickness and effective particle radius of clouds from reflected solar-radiation measurements. 1: Theory, *J. Atmos. Sci.*, *47* 1878–1893.

Peters, K., J. Quaas, and N. Bellouin (2011), Effects of absorbing aerosols in cloudy skies: A satellite study over the Atlantic Ocean, *Atmos. Chem. Phys.*, *11* 1393–1404, doi:10.5194/acp-11-1393-2011.

Petzold, A., M. Gysel, X. Vancassel, R. Hitzenberger, H. Puxbaum, S. Vrochticky, E. Weingartner, U. Baltensperger, and P. Mirabel (2005), On the effects of organic matter and sulphur-containing compounds on the CCN activation of combustion particles, *Atmos. Chem. Phys.*, *5*, 3187–3203, doi:10.5194/acp-5-3187-2005.

Petzold, A., J. Hasselbach, P. Lauer, R. Baumann, K. Franke, C. Gurk, H. Schlager, and E. Weingartner (2008), Experimental studies on particle emissions from cruising ship, their characteristic properties, transformation and atmospheric lifetime in the marine boundary layer, *Atmos. Chem. Phys.*, *8*, 2387–2403, doi:10.5194/acp-8-2387–2008.

Platnick, S., and S. Twomey (1994), Determining the susceptibility of cloud albedo to changes in droplet concentration with the Advanced Very High Resolution Radiometer, *J. Appl. Meteorol.*, *33*(3), 334–347.

Platnick, S., M. D. King, S. A. Ackerman, W. P. Menzel, B. A. Baum, J. C. Riédi, and R. A. Frey (2003), The MODIS cloud products: Algorithms and examples from Terra, *IEEE Trans. Geosci. Remote Sens.*, *41*(2), 459–473.

Pruppacher, H., and J. Klett (1997), *Microphysics of Clouds and Precipitation*, *Atmos. Oceanogr. Sci. Ser.*, vol. 18, 2nd ed., 954 pp., Kluwer Acad., Dordrecht, Netherlands.

Quaas, J., O. Boucher, and U. Lohmann (2006), Constraining the total aerosol indirect effect in the LMDZ and ECHAM4 GCMs using MODIS satellite data, *Atmos. Chem. Phys.*, *6*, 947–955, doi:10.5194/acp-6-947-2006.

Radke, L., J. Coakley, and M. King (1989), Direct and remote sensing observations of the effects of ships on clouds, *Science*, *246*(4934), 1146–1149.

Remer, L. A., et al. (2005), The MODIS aerosol algorithm, products, and validation, *J. Atmos. Sci.*, *62*, 947–973, doi:10.1175/JAS3385.1.

Remer, L. A., et al. (2008), Global aerosol climatology from the MODIS satellite sensors, *J. Geophys. Res.*, *113*, D14S07, doi:10.1029/2007JD009661.

Richter, A., V. Eyring, J. P. Burrows, H. Bovensmann, A. Lauer, B. Sierk, and P. J. Crutzen (2004), Satellite measurements of NO_2 from international shipping emissions, *Geophys. Res. Lett.*, *31*, L23110, doi:10.1029/2004GL020822.

Sandu, I., B. Stevens, and R. Pincus (2010), On the transitions in marine boundary layer cloudiness, *Atmos. Chem. Phys.*, *10*, 2377–2391, doi:10.5194/acp-10-2377-2010.

Schreier, M., H. Mannstein, V. Eyring, and H. Bovensmann (2007), Global ship track distribution and radiative forcing from 1 year of AATSR data, *Geophys. Res. Lett.*, *34*, L17814, doi:10.1029/2007GL030664.

Schreier, M., L. Joxe, V. Eyring, H. Bovensmann, and J. P. Burrows (2010), Ship track characteristics derived from geostationary satellite observations on the west coast of southern Africa, *Atmos. Res.*, *95*(1), 32–39, doi:10.1016/j.atmosres.2009.08.005.

Segrin, M. S., J. A. Coakley Jr., and W. R. Tahnk (2007), MODIS observations of ship tracks in summertime stratus off the west coast of the United States, *J. Atmos. Sci.*, *64*, 4330–4345, doi:10.1175/2007JAS2308.1.

Simmons, A. J., S. Uppala, D. Dee, and S. Kobayashi (2007), ERA-Interim: New ECMWF reanalysis products from 1989 onwards, *ECMWF Newsl. 110*, pp. 25–35, Euro. Cent. for Medium-Range Weather Forecasts, Reading, U. K.

Small, J. D., P. Y. Chuang, G. Feingold, and H. Jiang (2009), Can aerosol decrease cloud lifetime?, *Geophys. Res. Lett.*, *36*, L16806, doi:10.1029/2009GL038888.

Stevens, B., and G. Feingold (2009), Untangling aerosol effects on clouds and precipitation in a buffered system, *Nature*, *461*, 607–613, doi:10.1038/nature08281.

Teller, A., and Z. Levin (2006), The effects of aerosols on precipitation and dimensions of subtropical clouds: A sensitivity study using a numerical cloud model, *Atmos. Chem. Phys.*, *6*, 67–80, doi:10.5194/acp-6-67-2006.

Twomey, S. (1974), Pollution and the planetary albedo, *Atmos. Environ.*, *8*, 1251–1256.

Twomey, S., H. B. Howell, and T. A. Wojciechowski (1968), Comments on "Anomalous cloud lines," *J. Atmos. Sci.*, *25*, 333–334.

Wentz, F. J., and T. Meissner (2000), *AMSR Ocean Algorithm Theoretical Basis Document, Version 2*, report, Remote Sens. Syst., Santa Rosa, Calif.

Wielicki, B. A., B. R. Barkstrom, E. F. Harrison, R. B. Lee III, G. L. Smith, and J. E. Cooper (1996), Clouds and the Earth's Radiant Energy System (CERES): An Earth observing system experiment, *Bull. Am. Meteorol. Soc.*, *77*(5), 853–868.

Wood, R., and C. S. Bretherton (2004), Boundary layer depth, entrainment, and decoupling in the cloud-capped subtropical and tropical marine boundary layer, *J. Clim.*, *17*(18), 3576–3588.

H. Graßl and K. Peters, Max-Planck-Institut für Meteorologie, Bundesstr. 53, D-20146 Hamburg, Germany. (karsten.peters@ zmaw.de)

J. Quaas, Institute for Meteorology, University of Leipzig, Stephanstr. 3, D-04103 Leipzig, Germany.